Tellus
SERIES A
DYNAMIC
METEOROLOGY
AND OCEANOGRAPHY
PUBLISHED BY THE INTERNATIONAL METEOROLOGICAL INSTITUTE IN STOCKHOLM

*Tellus (2008), 60A, 1001–1022*
*Printed in Singapore. All rights reserved*



TELLUS

# Convection in Lorenz's global energy cycle with the ECMWF model

*By* MARTIN STEINHEIMER[1]*, MICHAEL HANTEL[1] and PETER BECHTOLD[2], [1]*Department of Meteorology and Geophysics, University of Vienna, Althanstraße 14, 1090 Vienna, Austria;* [2]*European Centre for Medium-Range Weather Forecasts, Reading, UK*

(Manuscript received 19 November 2007; in final form 14 May 2008)

ABSTRACT

Lorenz's global energy cycle includes the conversion rate $C$ between available potential and kinetic energy. In traditional estimates of $C$ only gridscale processes were evaluated; subgridscale processes were lumped into dissipation. It is argued that this is inadequate; organized subgridscale heat fluxes like deep convection cannot be treated as molecular.

Here both $C^{\mathrm{grid}}$ and $C^{\mathrm{sub}}$ are evaluated from the ECMWF Integrated Forecast System, for a 1-yr forecast in climate mode. The subgridscale fluxes are obtained from the model parametrization and the results tested for consistency; the largest contribution comes from the convection scheme. The integrand of $C^{\mathrm{sub}}$, the familiar 'buoyancy flux' $-\overline{\alpha'\omega'}$, is locally much smaller than its gridscale counterpart $-\overline{\alpha}\,\overline{\omega}$. However, the buoyancy flux is upward throughout, and thus representative for, the global atmosphere. The global annual means are $C^{\mathrm{grid}} = (3.4 \pm 0.1)\,\mathrm{W\,m^{-2}}$ and $C^{\mathrm{sub}} = (1.7 \pm 0.1)\,\mathrm{W\,m^{-2}}$. Further, the gridscale generation rate of available potential energy is evaluated independently and found to be $G^{\mathrm{grid}} = (3.0 \pm 0.2)\,\mathrm{W\,m^{-2}}$.

These results suggest that (i) the subgridscale processes contribute significantly to the Lorenz energy cycle and (ii) the cycle, represented by the total dissipation of $D = (5.1 \pm 0.2)\,\mathrm{W\,m^{-2}}$, is more intense than all earlier gridscale estimates have indicated.

## 1. Introduction

The concept of available potential energy of Lorenz (1955) describes the global energy cycle with the ultimate goal of quantifying the intensity of the general circulation of the atmosphere. However, only gridscale data have been used so far for evaluating the intensity of the circulation. Turbulent processes, including the important mechanisms of organized convection, have not been considered of any significance for the global energy cycle and thus have almost never been incorporated into the Lorenz exchange fluxes. It is the purpose of this study to provide evidence that subgridscale processes are of about the same relevance for the global energetics as are the traditional gridscale fluxes. The result will be that the global cycle is about twice as intense as thought so far.

The Lorenz energy cycle involves the reservoirs of available potential energy and kinetic energy, together with the related sources and sinks. The source for the available potential energy is the generation rate ($G$), while the kinetic energy is fed by the conversion rate ($C$) from available potential into kinetic energy, and diminished by the dissipation rate ($D$). All these quantities are understood as global climatological means. This implies that the reservoirs of available potential and kinetic energy are stationary. Hence, the fluxes $G$, $C$ and $D$ should be equal. Taken this equality for granted, the intensity of the general circulation can be specified by evaluating one of these three global mean flux quantities.

Classical data evaluations (Oort, 1964, 1983; Oort and Peixóto, 1983; Arpe et al., 1986; Peixóto and Oort, 1992) estimated $C$ from gridscale data. $G$ was also estimated, through employing the atmospheric heating rate and the efficiency factor, from gridscale data. The subgridscale effects were considered as molecular and lumped into dissipation. One prominent reason for this simplification was of a practical nature: The coarse data fields available for the early studies did not allow for the evaluation of subgridscale turbulent fluxes.

This state of affairs remained effective essentially up to today although subgridscale budget data have long become available. The basic philosophy in all existing numerical studies based on the Lorenz theory has been that subgridscale processes do not need to be explicitly considered. Why? One generally accepted reason has been that the kinetic energy of cloud-scale convection, presumably dissipated rapidly, does not represent useful work in the same class as large-scale atmospheric circulation.

*Corresponding author.
e-mail: martin@steinheimer.at
DOI: 10.1111/j.1600-0870.2008.00348.x

This attitude seems to be the tacit background of the more recent model and data evaluation studies in which a possible role of the subgridscale processes is not even mentioned (e.g. Siegmund, 1994; Rosen, 1999; Li et al., 2007; Boer and Lambert, 2008).

The philosophy to exclude the subgridscale processes from the global energy cycle is questionable since the cut between gridscale and subgridscale is necessarily arbitrary. The cut is no physical but a practical limit: It depends upon resolution of the data available. It is true that gridscale and subgridscale energy conversion processes are in different classes, that is, operate on space and time scales separated by some three or more orders of magnitude. However, only both types together represent the complete global energy cycle. It is in this sense that Hantel and Haimberger (2000) suggested to incorporate the subgridscale processes into the global energy cycle; their intention was not to improve the basic concept of Lorenz but rather to bring it to its completion.

Purpose of this study is to use the output from the ECMWF model for diagnosing both the gridscale and the subgridscale components of the energy cycle. In order to quantitatively calculate the source, conversion and sink rates, which are global integrals in the energy cycle, the first logical step is to diagnose the 'local patterns' of the corresponding integrands. These are quantities on a grid, representing averages over the corresponding grid cell, specified by the 3-D space-resolution and the time resolution of the data available; in the experiment of this study this is about 125 km in horizontal direction, 0.2–40 hPa in vertical direction, and about 1/2 h in time. Thus the second logical step is to discuss, not only the local energy equations that shall be applied for the budgets, but also the role of the 'finite grid size' and, as far as non-linear terms are involved, the corresponding correlation quantities over the grid cell which eventually show up as subgridscale quantities in the budget equations. The third logical step is then to calculate the 'global integrals' of the diagnosed gridscale quantities in order to come up with estimates of the corresponding global fluxes characteristic for the complete energy cycle.

Looking at the local gridscale ($-\overline{\alpha}\,\overline{\omega}$) and subgridscale ($-\overline{\alpha'\omega'}$) conversion rates, which will be introduced in Section 2 and are the integrands of the global mean conversion rate $C$, reveals that $-\overline{\alpha'\omega'}$ is locally negligible in size compared to $-\overline{\alpha}\,\overline{\omega}$. This has been another argument in favour of neglecting the small term $-\overline{\alpha'\omega'}$ altogether. The large gridscale $-\overline{\alpha}\,\overline{\omega}$, sometimes referred to as 'adiabatic term' (e.g. Bhatla et al., 2004), is positive in the tropics and negative in the subtropics, representing the Hadley cells on both hemispheres. These minima and maxima cancel each other almost completely in the global mean. In contrast, the locally quite small $-\overline{\alpha'\omega'}$ is positive practically throughout the entire atmosphere and thus suffers no cancellation. Following Haimberger and Hantel (2000) and Hantel et al. (2001) the quantity $-\overline{\alpha'\omega'}$ will also be referred to as the 'buoyancy flux'.

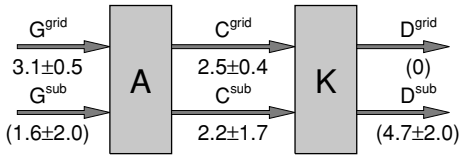


*Fig. 1.* Lorenz's global energy cycle generalized to include subgridscale processes. $A$ and $K$ are the reservoirs of available potential and kinetic energy, respectively. The traditional gridscale conversion rates are denoted $G^{\mathrm{grid}}$, $C^{\mathrm{grid}}$ and $D^{\mathrm{grid}}$. The corresponding new subgridscale conversion rates are $G^{\mathrm{sub}}$, $C^{\mathrm{sub}}$ and $D^{\mathrm{sub}}$. Values estimated assuming stationary reservoirs $A$ and $K$ are printed in parentheses (redrawn from Haimberger and Hantel, 2000).

Since high quality data from reanalysis projects carried out by NCEP/NCAR (Kalnay et al., 1996) and ECMWF (Uppala et al., 2005) have become available there should be no further need for excluding the integral of the buoyancy flux from the global energy budget. The time seems to be ripe for completing Lorenz's energy cycle through explicit implementation of the subgridscale processes. A first attempt into this direction has been made by Hantel and Haimberger (2000) and Haimberger and Hantel (2000), in the sequel cited as HH-I, HH-II. In these studies both generation rate $G$ and conversion rate $C$ were split into a gridscale ($G^{\mathrm{grid}}$, $C^{\mathrm{grid}}$) and a subgridscale fraction ($G^{\mathrm{sub}}$, $C^{\mathrm{sub}}$); the grid scale fractions correspond to Lorenz's classical $G$ and $C$. Concerning $D$ it was assumed that dissipation, which is a molecular process, occurs only on the smallest scales and thus is completely described by $D^{\mathrm{sub}}$ while $D^{\mathrm{grid}}$ should be zero.

The evaluations of HH-II suggest that the subgridscale conversion rate $C^{\mathrm{sub}}$ is of about equal size as the gridscale conversion rate $C^{\mathrm{grid}}$. This implies that the global energy cycle is about twice as efficient as has been known from the classical evaluations. Figure 1 presents the results achieved by HH-II. The reason why HH-II focused strongly on the conversion rate was that evaluating the two components of $C$ is a quite transparent task, as opposed to $G$ which is more involved. The local fields $-\overline{\alpha}\,\overline{\omega}$ and $-\overline{\alpha'\omega'}$ can be diagnosed and the corresponding global averages $C^{\mathrm{grid}}$ and $C^{\mathrm{sub}}$ can be determined by mass integration. This study will also primarily be focused on these two components of the conversion rate $C$. Concerning the generation rate only the gridscale component $G^{\mathrm{grid}}$ can be evaluated while the subgridscale component $G^{\mathrm{sub}}$ cannot.

The studies HH-I, HH-II were limited by the fact that the subgridscale conversion rate had to be estimated with a quite preliminary method. Consequently, the estimates of HH-II had an error of almost 80% for $C^{\mathrm{sub}}$.

The method adopted in this study is to draw the gridscale quantities required from ECMWF's weather prediction model Integrated Forecast System (IFS). Further, the most relevant subgridscale quantities that hitherto have been missing in the Lorenz's energy cycle will be inferred from the parametrization schemes of the IFS. This can be made in a consistent manner and with much improved accuracy.

The data used in this study will be extracted from a 1-yr forecast in climate mode of the IFS started from 1 August 2000. The routinely stored fields as well as special fields from the parametrization schemes will be employed. While $-\overline{\alpha}\,\overline{\omega}$ is explicitly contained in the model's temperature budget equation and can be calculated from gridscale fields, $-\overline{\alpha'\omega'}$ is neglected in the temperature budget equation of the IFS. However, the buoyancy flux can be calculated from the subgridscale fluxes of temperature and specific humidity (Section 2). The divergences of these fluxes play an important role in the forecast equations of temperature and specific humidity and are therefore explicitly included in the parametrization of the model. How these fluxes are extracted from the corresponding schemes is presented in Section 4. The pertinent details of the model run are presented in Section 5.

In his consideration of the cumulus parametrization problem Arakawa (2004) discusses the notion pairs gridscale/subgridscale and resolved/unresolved as opposed to large-scale/cumulus scale and observed/non-observed. He points out that in diagnostic studies of cumulus effects based on observed large-scale budgets (e.g. Yanai and Johnson, 1993) the density of the observation network separates observed and non-observed processes and maintains that 'finding a cause-and-effect relationship should not be an issue' in such a study. This is also the philosophy of the present investigation. The parametrized fluxes of the IFS will be used as substitutes for the unobserved subgridscale (in short: convective) processes in the atmosphere. While the convective processes go unobserved they nevertheless have a deep impact, not only upon the forecast fields, but upon the global energy budget as well. To extract them from the IFS is a matter of practical convenience. However, no statement concerning a possible cause-and-effect relationship is intended in this study.

This will be advantageous from another perspective: The notion subgridscale comprises processes that are so different as are anisotropic penetrative cumulus convection and isotropic boundary layer convection. As again Arakawa (2004) points out the statistical distributions of dynamical and thermodynamic properties of air in the cloudy atmosphere are highly skewed; following Arakawa, the concepts of 'mean and variance' are less useful than those of 'environment and cloud'. While the latter distinction is indispensable when it comes to closure and parametrization the formal notion pair mean/variance, expressed here as gridscale/subgridscale, is the only way to lump physically different unresolved processes into one unifying category.

The straightforward 'mean-and-variance' method will nevertheless reveal that the subgridscale buoyancy flux is most pronounced in the latitudes of the intertropical convergence zone (ITCZ) where penetrative cumulus convection is dominant; the buoyancy flux is less dominant, while still relevant, in the boundary layer where convection tends to be isotropic. Both mechanisms are physically different. Yet both are of 'convective' nature and both are controlled by buoyancy; thus it may seem admissible to apply the notion 'subgridscale' in equal manner for both.

The use of the parametrized output does not necessarily reproduce the energy budget of the IFS. For example, the interaction between subgridscale potential and eddy kinetic energy through the buoyancy flux, a key process in the turbulence kinetic energy equation (Stull, 1988), is actually not reproduced in the present implementation of the IFS. This does however not prevent the IFS to be energetically consistent, since only the gridscale energy reservoirs are considered in the model.

Finally, no attempt will be made in this paper to advance in any way the physical background of Lorenz's energy cycle. There have been various studies in the past that have investigated further theoretical aspects of the Lorenz theory. For example, Johnson (2000) considers in his review article (see also citations therein) the relations between the energy budget and the entropy budget and points to a widespread misconception 'that available potential energy, once generated, is the spring which drives atmospheric circulations'. This study does not try to get involved in these discussions but will be satisfied with accepting the global energy budget in Lorenz's classical form. The only innovative aspect will be to discuss the convective component. This component has been implicitly contained in the Lorenz cycle from the beginning but has been tacitly suppressed by practically all subsequent data evaluations. The purpose of this study is to diagnose this missing component and to demonstrate its relevance.

## 2. Local energy equations

Since total energy cannot objectively be separated into parts (van Mieghem, 1973; Falk and Ruppel, 1976) the separation of total energy into kinetic and internal energy is ambiguous. The same applies to the exchange between these arbitrarily chosen energy forms. In HH-I three equivalent sets of local equations of thermodynamic and mechanical energy were discussed; the authors decided that the most useful for numerical evaluation is the one suggested by Lorenz (1967). Using standard Cartesian tensor notation ($T$ = temperature, $p$ = pressure, $\alpha$ = specific volume, $\omega = \mathrm{d}p/\mathrm{d}t$, $\Phi$ = geopotential, $k$ = 3-D kinetic energy, $\pi_{ij}$ = tensor of molecular momentum flux, $\varepsilon$ = local dissipation, $s$ = specific entropy, $Q = T\,\mathrm{d}s/\mathrm{d}t$ = net heating and $c_p$ = specific heat at constant pressure) this set of equations reads:

$$\frac{\mathrm{d}a}{\mathrm{d}t} = NQ + \alpha\omega \tag{1}$$

$$\frac{\mathrm{d}b}{\mathrm{d}t} + \alpha\frac{\partial}{\partial x_j}(pv_j + \pi_{ij}v_i) = -\alpha\omega - \varepsilon. \tag{2}$$

The state quantities are defined as:

$$a \equiv Nc_pT + P \tag{3}$$

$$b \equiv k + \Phi - p\alpha. \tag{4}$$

Definition of the efficiency factor $N$ follows Lorenz (1967) and Boer (1975):

$$N \equiv 1 - (p_r/p)^{\kappa} \tag{5}$$

$$\frac{\mathrm{d}N}{\mathrm{d}t} = -\kappa(1-N)\left(\frac{1}{p_r}\frac{\mathrm{d}p_r}{\mathrm{d}t} - \frac{\omega}{p}\right), \tag{6}$$

where $p_r$ is a barotropic reference pressure chosen otherwise arbitrarily except for the condition that the global mean of $N$ is zero; $\kappa = R_a/c_p$($R_a$= gas constant of dry air). The potential $P$ is a function of potential temperature $\theta$ specified by:

$$\mathrm{d}P(\theta) = R_a\theta\left[\frac{p_r(\theta)}{p_0}\right]^{\kappa}\frac{1}{p_r(\theta)}\mathrm{d}p_r(\theta). \tag{7}$$

For this set of equations the local conversion rate between kinetic and potential energy is the flux $-\alpha\omega$, on the gridscale to be understood as $-\overline{\alpha}\,\overline{\omega}$. The gridscale adiabatic term $-\overline{\alpha}\,\overline{\omega}$ can be calculated from gridscale data archived operationally by GCMs (global circulation models) but the subgridscale buoyancy flux $-\overline{\alpha'\omega'}$ is not available. However, this correlation quantity, by substituting $\alpha$ using the gas law and virtual temperature $T_v$, can be transformed into:

$$-\overline{\alpha'\omega'} = -\left[\frac{R_a}{p} + \frac{(R_v - R_a)\overline{q_v}}{p}\right]\overline{T'\omega'} - \frac{(R_v - R_a)\overline{T}}{p}\overline{q_v'\omega'}, \tag{8}$$

where $R_v$ is the gas constant of water vapour and $q_v$ is specific humidity. The liquid water fraction of the air was neglected as well as pressure perturbations and triple correlations. Following Hantel et al. (1993) the turbulent fluxes of sensible heat ($w = c_p g^{-1}\,\overline{T'\omega'}$) and latent heat ($f = L_v g^{-1}\,\overline{q_v'\omega'}$, $L_v$ = condensation heat) are introduced. This turns eq. (8) into:

$$-\overline{\alpha'\omega'} = -\frac{g}{p}\left[\frac{R_a}{c_p} + \frac{(R_v - R_a)\overline{q_v}}{c_p}\right]w - \frac{g}{p}\frac{(R_v - R_a)\overline{T}}{L_v}f. \tag{9}$$

To estimate the buoyancy flux with this formula the turbulent fluxes $w$ and $f$ can be diagnosed from gridscale budgets as has been done in HH-II, or extracted from parametrization as will be done in this study.

In HH-II the budget equation of moist enthalpy was used to diagnose the 'total convective heat flux' ($c = w + f$) from reanalysis data of NCEP/NCAR (Kalnay et al., 1996) and ECMWF (Uppala et al., 2005). To get the fluxes $w$ and $f$ separately, the Bowen ratio ($w/f$) was specified externally. This closure assumption has been the drawback of the method used in HH-II. The specification of the Bowen ratio profile is largely arbitrary, since neither this quantity nor $w$ nor $f$ separately are routinely observed.

A further point in HH-II was how to diagnose the integrand of the generation rate. For this purpose the Lorenz net heating was equated to the 'response', a quantity defined as follows:

$$Q = \frac{\mathrm{d}c_pT}{\mathrm{d}t} - \alpha\omega = R. \tag{10}$$

The heating $Q = T\,\mathrm{d}s/\mathrm{d}t$ comprises reversible and irreversible contributions from the processes of radiation, phase changes, dissipation (due to local velocity gradients), heat conduction (due to local temperature gradients) and diffusion (due to local concentration gradients). However, it has been impossible to estimate $Q$ from these actual physical processes; the reason is that this approach would be too inaccurate (see, e.g. the early attempts by Newell et al., 1970). Rather, $Q$ has been estimated in HH-II from the dry enthalpy eq. (10) in form of the 'response' $R$. This quantity is defined on the gridscale as follows:

$$\overline{R} = \underbrace{c_p\frac{\partial\overline{T}}{\partial t} + c_p\nabla_2\cdot\overline{T}\,\overline{V_2} + c_p\frac{\partial\overline{T}\,\overline{\omega}}{\partial p} - \overline{\alpha}\,\overline{\omega}}_{\overline{R}^{\mathrm{grid}}} + \underbrace{c_p\frac{\partial\overline{T'\omega'}}{\partial p} - \overline{\alpha'\omega'}}_{\overline{R}^{\mathrm{sub}}}. \tag{11}$$

This setting will enable us to estimate the components $\overline{R}^{\mathrm{grid}}$, $\overline{R}^{\mathrm{sub}}$ of the generation rate.[1]

## 3. Conversion and generation rates

From the local quantities the corresponding global generation and conversion fluxes as defined by Lorenz are gained as global mass averages (indicated by curly brackets in this paper). This yields the global conversion rate $C = \{-\alpha\omega\}$. If the conversion rate is split into a local average (denoted by an overbar) over a pertinent space/time interval (one gridbox in the model) and the deviation from this mean (indicated by a prime) its global mass average yields:

$$C = C^{\mathrm{grid}} + C^{\mathrm{sub}} = \{-\overline{\alpha}\,\overline{\omega}\} + \left\{-\overline{\alpha'\omega'}\right\}. \tag{12}$$

Despite the limitations of the method applied in HH-II, this study nevertheless demonstrated that $C^{\mathrm{sub}}$ is positive and not negligible in size compared to $C^{\mathrm{grid}}$. The diagnosed results of this preliminary work, with an estimated error of about 80% for $C^{\mathrm{sub}}$, are reproduced in Fig. 1.

With the concept of the response $R$ the generation rate components are defined as:

$$G^{\mathrm{grid}} = \{\overline{N}\,\overline{R}\}; \qquad G^{\mathrm{sub}} = \{\overline{N'R'}\}. \tag{13}$$

[1] The flux $\overline{T'\omega'}$ is zero at the earth's surface. It diverges in the less than 1 cm thick skin layer above the surface. The molecular sensible heat flux converges from the surface flux to zero at the top of the skin layer (cf. HH-II). This distinction is only relevant for the calculation of $\overline{R}^{\mathrm{sub}}$, while otherwise the molecular sensible heat flux is included in $w$.

Since both $\overline{N}$ and $\overline{R}$ can be extracted from model data, the gridscale conversion rate $G^{\text{grid}}$ is readily accessible and has been included in Fig. 1. On the other hand, neither $N'$ nor $R'$ are accessible from model data and thus, as already noted by HH-II, $G^{\text{sub}}$ cannot be independently diagnosed.

In the early evaluations of the Lorenz global cycle the conversion rate was not calculated in the '$\alpha\omega$-formulation' but in the hydrostatically equivalent '$V$ grad $\Phi$-formulation' (e.g. Oort and Rasmusson, 1971; Peixóto and Oort, 1992). This seems to be an issue even in recent evaluations (e.g. Li et al., 2007). For selected cases (not shown in detail here) both formulations were applied; it was found that, for the global average, both yield identical results within error margins. For this reason the '$V$ grad $\Phi$-formulation' was abandoned; the '$\alpha\omega$-formulation' was exclusively employed.

## 4. Isolating the buoyancy flux from the IFS

In order to gain the buoyancy flux by means of eq. (9) the central task is to extract $w$ and $f$ from the IFS. The gridscale forecast equations are discussed first, followed by the parametrized tendencies involved.

### 4.1. The forecast equations

Gridscale state quantities, carried in the IFS as prognostic variables, are, among others, temperature $\overline{T}$, specific humidity $\overline{q_v}$, and cloud water $\overline{q_{li}}$ (indices $l$, $i$ for liquid water and ice). The tendencies of the first two are gained from the following forecast equations in $\eta$-coordinates (Ritchie et al., 1995):

$$\frac{\partial \overline{T}}{\partial t} = -\left(\overline{V}_2 \cdot \nabla_2 \overline{T} + \overline{\dot{\eta}} \frac{\partial \overline{T}}{\partial \eta} - \frac{\overline{\alpha}\,\overline{\omega}}{c_p}\right) + P_T + K_T \tag{14}$$

$$\frac{\partial \overline{q_v}}{\partial t} = -\left(\overline{V}_2 \cdot \nabla_2 \overline{q_v} + \overline{\dot{\eta}} \frac{\partial \overline{q_v}}{\partial \eta}\right) + P_q + K_q. \tag{15}$$

Notation is standard, the index 2 denotes horizontal wind and horizontal nabla operator. $P_T$ and $P_q$ comprise the contributions of the parametrization; $K_T$ and $K_q$ stand for horizontal diffusion. In the current model implementation no horizontal diffusion is applied to specific humidity, hence $K_q$ is neglected and will be dropped from here on. Further, in the present experiment $K_T$ was stored, together with other terms, in the quantity $\partial T/\partial t|_{\text{remain}}$ (see Table 2), so $K_T$ will not be explicitly visible in the subsequent equations. Likewise the small buoyancy flux $-\overline{\alpha'\omega'}$ does not explicitly show up in eq. (14) because it is for the most part balanced by dissipation which is included in $P_T$ in a correspondingly reduced form.

The terms in parentheses are understood as advection in spherical coordinates with vertical hybrid coordinate $\eta$ (Simmons and Burridge, 1981). The advection is calculated using a semi-Lagrangian method and the thermodynamic eq. (14) is solved semi-implicitly. For details of the algorithm see Ritchie et al. (1995) and Hortal (2002).

The terms $P_T$ and $P_q$ are split into apparent tendencies from the various parametrization schemes in the IFS (diffusion 'diff', convection 'conv', cloud 'cloud', and radiation 'rad'):[2]

$$P_T = \left.\frac{\partial T}{\partial t}\right|_{\text{diff}} + \left.\frac{\partial T}{\partial t}\right|_{\text{conv}} + \left.\frac{\partial T}{\partial t}\right|_{\text{cloud}} + \left.\frac{\partial T}{\partial t}\right|_{\text{rad}} \tag{16}$$

$$P_q = \left.\frac{\partial q_v}{\partial t}\right|_{\text{diff}} + \left.\frac{\partial q_v}{\partial t}\right|_{\text{conv}} + \left.\frac{\partial q_v}{\partial t}\right|_{\text{cloud}}. \tag{17}$$

The temperature tendency due to gravity wave drag processes used to be calculated in a separate scheme in the IFS. However, effective since the IFS Cycle 31R1, a common solver for temperature diffusion and turbulent orographic form drag (gravity wave drag) has been introduced. The last term in (16) describes the heat sources due to radiation; it acts only upon temperature, not upon specific humidity or condensate.

The buoyancy flux will be gained by extracting the turbulent heat flux $w$ from (16) and the turbulent heat flux $f$ from (17) and substituting $w$ and $f$ into eq. (9).

### 4.2. Apparent tendencies in the IFS

The model eqs (14) and (15) can now be recast in the following symbolic form:

$$\frac{\partial \overline{T}}{\partial t} = \left.\frac{\partial T}{\partial t}\right|_{\text{dyn}} + P_T \tag{18}$$

$$\frac{\partial \overline{q_v}}{\partial t} = \left.\frac{\partial q_v}{\partial t}\right|_{\text{dyn}} + P_q. \tag{19}$$

The gridscale tendencies on the left-hand side are composed of the contributions of the gridscale processes (subscript 'dyn' for 'dynamic terms', equivalent to the quantities in parentheses in the forecast equations) and of the contributions $P_T$, $P_q$ of non-gridscale processes to be parametrized according to eqs (16) and (17).

It should be stressed that only the left-hand sides of these equations are real tendencies like, for example, the partial derivative of $\overline{T}$ with respect to time. The terms on the right-hand side of eqs (18) and (19), on the other hand, represent different contributions to the tendencies which, however, are no tendencies by themselves. This has been indicated by suppressing the overbar on the terms on the right-hand sides. For example, there is no quantity like $T_{\text{dyn}}$ that could be gained by independently integrating $(\partial T/\partial t)|_{\text{dyn}}$ with respect to time. Rather, the expression

[2] The expression 'diffusion scheme', used in daily parlance, comprises not only molecular diffusion but includes also mass-flux contributions and dissipation. Its full name reads 'turbulent transport and interaction with the surface' (ECMWF, 2007). For simplicity the subscript 'diff' in eqs (16) and (17) will be kept here.

$(\partial T/\partial t)|_{\rm dyn}$ is to be considered as an 'apparent tendency'. Each one of these apparent tendencies in eqs (18) and (19) is a shorthand notation for the complex processes that yield a certain contribution to the true tendency $\partial\overline{T}/\partial t$ of the gridscale state quantity $\overline{T}$.

These processes can be of a quite different nature. For example, the processes represented by $(\partial\, T/\partial\, t)|_{\rm dyn}$ describe transformations of gridscale quantities; on the other hand, the processes represented by $P_T$, $P_q$ specified in eqs (16) and (17) describe parametrizations of subgridscale contributions.

### 4.3. Calculating the turbulent fluxes

The ECMWF parametrization involves, among other processes not discussed here, phase changes and turbulent fluxes. The phase changes are transformations between reservoirs of state quantities and require careful observation of budget laws. The turbulent fluxes, on the other hand, are the ones to be isolated. This complex parametrization task is implemented in the IFS in form of the following schemes (ECMWF, 2007):

(i) The 'diffusion scheme' models boundary-layer and free atmospheric vertical diffusion, transport and microphysics in stratocumulus clouds, as well as kinetic energy dissipation through gravity wave and surface drag.

(ii) The 'convection scheme' calculates convective cloud and transport processes. In addition, it communicates with the stratiform cloud scheme through the detrainment of cloud water and ice.

(iii) The 'cloud scheme' computes cloud fraction, precipitation and microphysical phase changes in stratiform clouds; no turbulent fluxes are included.

For the exchange between the state quantities specific humidity $\overline{q_v}$, cloud water $\overline{q_l}$, $\overline{q_i}$ and precipitation water $\overline{q_r}$, $\overline{q_s}$ there are four phase change terms in each corresponding budget equation. These generate eight heating terms in the temperature equation. Four are caused by condensation/sublimation of water vapour and the remaining four are caused by the freezing/melting transition from $q_l, q_r$ to $q_i, q_s$. They will be included in the temperature equation through the two terms with the superscripts $v \leftrightarrow lirs$ (four phase fluxes between vapour and condensed water) and $lr \leftrightarrow is$ (another four phase fluxes between the liquid and the frozen phase of water). This reads for the diffusion scheme and the convection scheme in the temperature forecast equation:

$$\left.\frac{\partial T}{\partial t}\right|_{\rm diff} = \left.\frac{\partial T}{\partial t}\right|_{\rm diff}^{\rm turb} + \left.\frac{\partial T}{\partial t}\right|_{\rm diff}^{v\leftrightarrow lirs} + \left.\frac{\partial T}{\partial t}\right|_{\rm diff}^{lr\leftrightarrow is} + \left.\frac{\partial T}{\partial t}\right|_{\rm diff}^{diss} + \left.\frac{\partial T}{\partial t}\right|_{\rm diff}^{gw}; \tag{20}$$

$$\left.\frac{\partial T}{\partial t}\right|_{\rm conv} = \left.\frac{\partial T}{\partial t}\right|_{\rm conv}^{\rm turb} + \left.\frac{\partial T}{\partial t}\right|_{\rm conv}^{v\leftrightarrow lirs} + \left.\frac{\partial T}{\partial t}\right|_{\rm conv}^{lr\leftrightarrow is}; \tag{21}$$

and for gaseous specific humidity:

$$\left.\frac{\partial q_v}{\partial t}\right|_{\rm diff} = \left.\frac{\partial q_v}{\partial t}\right|_{\rm diff}^{\rm turb} + \left.\frac{\partial q_v}{\partial t}\right|_{\rm diff}^{v\leftrightarrow lirs}; \tag{22}$$

$$\left.\frac{\partial q_v}{\partial t}\right|_{\rm conv} = \left.\frac{\partial q_v}{\partial t}\right|_{\rm conv}^{\rm turb} + \left.\frac{\partial q_v}{\partial t}\right|_{\rm conv}^{v\leftrightarrow lirs}. \tag{23}$$

Note that the phase fluxes $lr \leftrightarrow is$ concern only the apparent tendency of temperature. The cloud scheme contains no turbulent contribution and thus does not need to be discussed here (see Table 4 in Section A.1).

Contributions to the apparent tendencies due to turbulence come from the diffusion and the convection scheme (not from the cloud scheme). This yields:

$$\begin{aligned}\left.\frac{\partial T}{\partial t}\right|^{\rm turb} &= \left.\frac{\partial T}{\partial t}\right|_{\rm diff}^{\rm turb} + \left.\frac{\partial T}{\partial t}\right|_{\rm conv}^{\rm turb}\\ \left.\frac{\partial q_v}{\partial t}\right|^{\rm turb} &= \left.\frac{\partial q_v}{\partial t}\right|_{\rm diff}^{\rm turb} + \left.\frac{\partial q_v}{\partial t}\right|_{\rm conv}^{\rm turb}.\end{aligned} \tag{24}$$

The convective contributions are by far the largest ones; the diffusive terms are generally much smaller. Yet the diffusive terms can for principal reasons not be neglected; they couple the free atmosphere fluxes to the molecular heat exchange across the earth's surface and, when neglected, cause severe inconsistencies in the fluxes of sensible and latent heat.

The parametrized tendencies in the IFS can be interpreted in the sense that the only components that contribute to the subgridscale fluxes $w, f$ are the four apparent tendencies with superscript 'turb'; they are represented in eq. (24). Thus the first step to obtain $w, f$ from the tendencies is to define the 'kinematic temperature fluxes' $F^T_{\rm diff}$, $F^T_{\rm conv}$ through:

$$-g\frac{\partial F^T_{\rm diff}}{\partial p} = \left.\frac{\partial T}{\partial t}\right|_{\rm diff}^{\rm turb}; \qquad -g\frac{\partial F^T_{\rm conv}}{\partial p} = \left.\frac{\partial T}{\partial t}\right|_{\rm conv}^{\rm turb}. \tag{25}$$

In similar manner 'the kinematic moisture fluxes' $F^{q_v}_{\rm diff}$, $F^{q_v}_{\rm conv}$ are defined through:

$$-g\frac{\partial F^{q_v}_{\rm diff}}{\partial p} = \left.\frac{\partial q_v}{\partial t}\right|_{\rm diff}^{\rm turb}; \qquad -g\frac{\partial F^{q_v}_{\rm conv}}{\partial p} = \left.\frac{\partial q_v}{\partial t}\right|_{\rm conv}^{\rm turb}. \tag{26}$$

The fluxes $F$ are gained from the corresponding tendencies, which are functions of pressure, through straight vertical mass integration plus observing that there is no material flux across the top of the atmosphere ($p = 0$), for example:

$$F^T_{\rm diff}(p) = -\frac{1}{g}\int_{p'=0}^{p'=p}\left(\left.\frac{\partial T}{\partial t}\right|_{\rm diff}^{\rm turb}\right){\rm d}p'. \tag{27}$$

From the kinematic fluxes the convective heat and moisture fluxes are obtained as:

$$w(p) = c_p\left(F^T_{\rm diff} + F^T_{\rm conv}\right); \quad f(p) = L_v\left(F^{q_v}_{\rm diff} + F^{q_v}_{\rm conv}\right). \tag{28}$$

Both $w$ and $f$, like the kinematic fluxes, are functions of pressure within the column over which the mass integration (27) has been

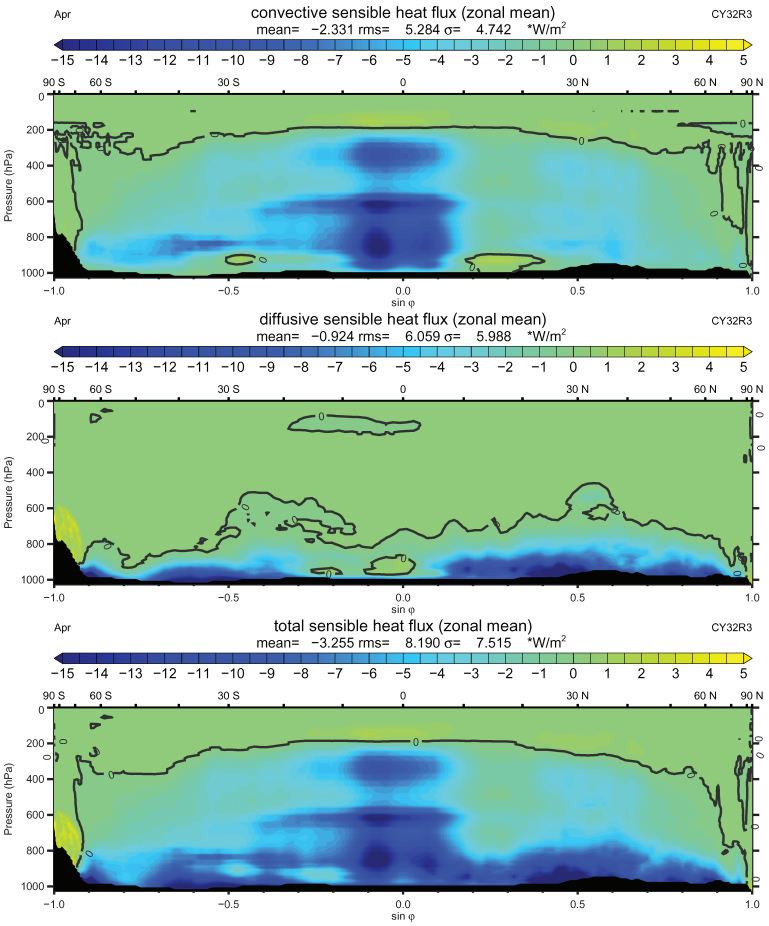


*Fig. 2.* Zonal mean of the contributions to the sensible heat flux from convection (kinematic flux $F^T_{\rm conv}$, upper picture) and diffusion scheme (kinematic flux $F^T_{\rm diff}$, middle) and their sum $w$ (lower picture) according to eq. (28). Valid for April of the climate run.

carried out. In addition, of course, all are functions of time and of the position of the column, that is, of the horizontal coordinates.

Figures 2 and 3 show the kinematic fluxes $F^T_{\rm conv}$, $F^T_{\rm diff}$, $F^{q_v}_{\rm conv}$, $F^{q_v}_{\rm diff}$ and their respective sums for the month of April.[3] These represent the basic information required for diagnosing the field of the buoyancy flux. Only the two that are yielded by the convection scheme are explicitly available: $F^T_{\rm conv}$ and $F^{q_v}_{\rm conv}$. The two diffusive fluxes $F^T_{\rm diff}$ and $F^{q_v}_{\rm diff}$ are not explicitly available but have to be calculated from the corresponding tendencies. The necessary formulae are assembled in Section A.2.

### 4.4. *Numerical implementation of the flux algorithm*

The right-hand sides of the relations (25), (26) are usually understood as vertical averages over model layers and considered as valid on full model levels $\eta_k$. For example, in the IFS eq. (27) may be generalized to the vertical integral between half model levels $\eta_{k-\frac{1}{2}}$, $\eta_{k+\frac{1}{2}}$:

$$-\frac{1}{g}\int_{p(\eta_{k-\frac{1}{2}})}^{p(\eta_{k+\frac{1}{2}})} \left.\frac{\partial T}{\partial t}\right|^{\rm turb} {\rm d}p = \int_{p(\eta_{k-\frac{1}{2}})}^{p(\eta_{k+\frac{1}{2}})} \frac{\partial F^T(p)}{\partial p}\,{\rm d}p. \qquad (29)$$

The integrations are carried out over pressure. Since the integrands are also functions of time $t$ and of the horizontal coordinates $\lambda$, $\varphi$ it follows:

$$-\frac{1}{g}\left.\frac{\partial T}{\partial t}\right|^{\rm turb} \Delta p = F^T(t,\lambda,\varphi,\eta_{k+\frac{1}{2}}) - F^T(t,\lambda,\varphi,\eta_{k-\frac{1}{2}}). \qquad (30)$$

The left-hand side of this equation is a function of $t$, $\lambda$, $\varphi$, $\eta_k$; it is defined at every grid cell in the IFS. Note that $\Delta p$ is generally not constant between constant half levels $\eta_{k-\frac{1}{2}}$, $\eta_{k+\frac{1}{2}}$ (neither in time nor in space). Equation (30) yields, with boundary condition $F^T(t,\lambda,\varphi,0)$=0, the vertical profile of $F^T$ at every time step and at every geographical position. It can be integrated with respect to time to yield the accumulated flux; likewise, it can be integrated horizontally with respect to $\lambda$, $\varphi$ to yield the global average of $F^T$ on the respective $\eta$-level.

[3] Basic statistics (mean, rms, $\sigma$) are printed in the header of each plot. For zonal means (like Fig. 2) this applies to the complete 3-D field; for horizontal geographical maps (like Fig. 5) this applies to the field displayed.

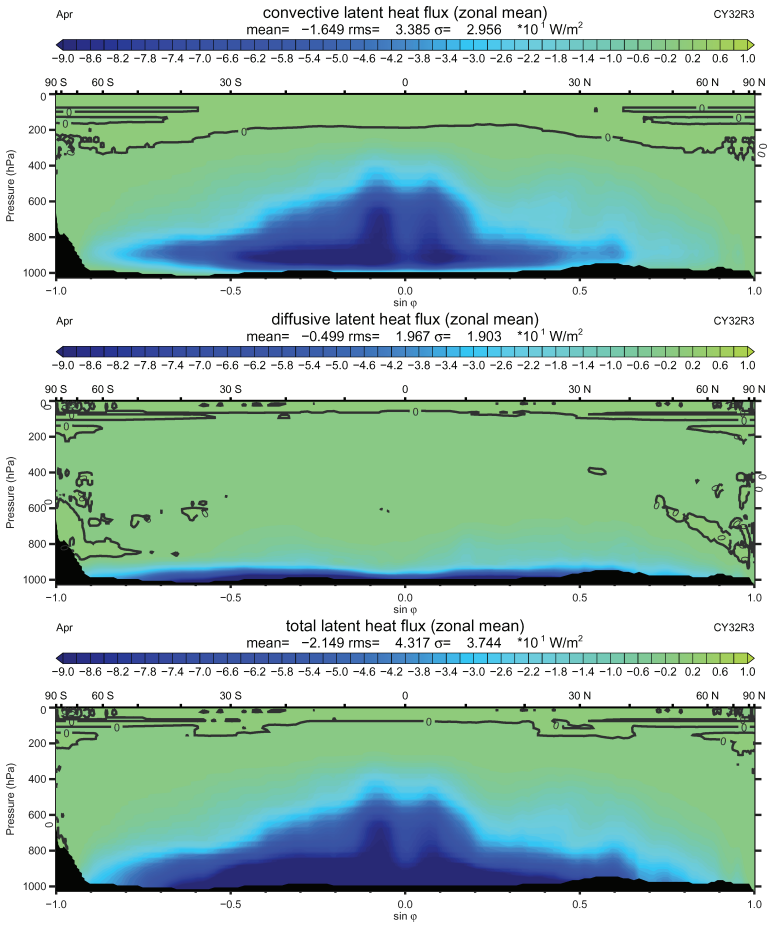


*Fig. 3.* Zonal mean of the contributions to the latent heat flux from convection (kinematic flux $F^{q_v}_{\text{conv}}$, upper picture) and diffusion scheme (kinematic flux $F^{q_v}_{\text{diff}}$, middle) and their sum $f$ (lower picture) according to eq. (28). Valid for April of the climate run.

### *4.5. Archiving temporal mean fluxes/tendencies*

It is common practice at ECMWF to archive time integrated tendencies and fluxes for data evaluation from forecast runs. This is the appropriate implementation to investigate local tendencies of state variables.

However, for the evaluation of energy budgets as intended in this study it is essential to account for the temporal mass variations of the model layers; that is, variations of $\Delta p$. This is implemented here by archiving time integrated tendencies weighted by the layer thickness $\Delta p$. Integrating (30) over time shows that only these weighted tendencies are consistent with the time integrated fluxes.

The global gridscale conversion rate $C = \{-\overline{\alpha}\,\overline{\omega}\}$ is most sensitive to mass variations. When it is calculated by time integration and following mass integration the result is 5.1 W m$^{-2}$, while the accurate result from mass integration followed by time integration is 3.4 W m$^{-2}$. In order to guarantee correct temporal mass means and consistency between tendencies and fluxes this study deviates from ECMWF standard in that mass weighted tendencies were archived. Only in Section 6.1 the standard ECMWF archiving mode was used.

## 5. Model setup

In this study monthly mean parametrized tendencies/fluxes were extracted from a 1-yr forecast run of the IFS (Cycle 32R3). The spectral resolution used was T159 corresponding to a reduced Gaussian grid with an approximate distance between gridpoints of 125 km. In the vertical 60 hybrid model layers were used. The time step used was 0.5 h.[4]

The integrations were initialized from the ERA40; they used analysed sea surface temperatures. The annual model integrations were checked against ERA40 and surface and satellite observations. The results were in reasonable agreement; a long-term drift in the model state can be excluded. In addition to the parametrized tendencies/fluxes used to calculate $w$ and $f$ all tendencies necessary to reproduce the local tendencies of temperature and specific humidity using the respective budget equation were extracted from the model run.

The model fields used in this study are assembled in Tables 1 and 2. Table 1 lists the fields that are routinely stored for every

[4] A run with 1-h time step was also made with much the same results (not shown).

*Table 1.* Fields routinely stored in the IFS for every operational model run

| Name | Unit | Field |
|---|---|---|
| $T$ | [K] | Temperature |
| $q_v$ | | Specific humidity |
| $\langle PREC_{\text{cloud}} \rangle$ | [m] | Accumulated surface large scale precipitation |
| $\langle PREC_{\text{conv}} \rangle$ | [m] | Accumulated surface convective precipitation |
| $\langle SH \rangle$ | [W m$^{-2}$*s] | Accumulated surface sensible heat flux |
| $\langle LH \rangle$ | [W m$^{-2}$*s] | Accumulated surface latent heat flux |

*Note:* For definition of operator $\langle\rangle$ see eq. (31).

*Table 2.* Special fields stored within the present experiment in addition to the routinely stored fields

| Name | Unit | Accumulated tendencies due to |
|---|---|---|
| $\left\langle \frac{\partial T}{\partial t}\big\vert_{\text{dyn}} \Delta p \right\rangle$ | $\left[\frac{K\,Pa}{s}\,s\right]$ | Dynamics including $\overline{\alpha}\,\overline{\omega}/c_p$ |
| $\langle \frac{\partial T}{\partial t}\big\vert_{\overline{\alpha}\,\overline{\omega}} \Delta p \rangle$ | $\left[\frac{K\,Pa}{s}\,s\right]$ | $\overline{\alpha}\,\overline{\omega}/c_p$ separately |
| $\left\langle \frac{\partial T}{\partial t}\big\vert_{\text{diff},*} \Delta p \right\rangle$ | $\left[\frac{K\,Pa}{s}\,s\right]$ | Diffusion scheme (without turbulent orographic form drag and boundary layer dissipation) |
| $\langle \frac{\partial T}{\partial t}\big\vert_{\text{conv}} \Delta p \rangle$ | $\left[\frac{K\,Pa}{s}\,s\right]$ | Convection scheme |
| $\langle \frac{\partial T}{\partial t}\big\vert_{\text{cloud}} \Delta p \rangle$ | $\left[\frac{K\,Pa}{s}\,s\right]$ | Cloud scheme |
| $\langle \frac{\partial T}{\partial t}\big\vert_{\text{rad}} \Delta p \rangle$ | $\left[\frac{K\,Pa}{s}\,s\right]$ | Radiation scheme |
| $\langle \frac{\partial T}{\partial t}\big\vert_{\text{remain}} \Delta p \rangle$ | $\left[\frac{K\,Pa}{s}\,s\right]$ | horizontal diffusion $K_T$, turbulent orographic form drag, boundary layer dissipation |
| $\left\langle \frac{\partial q_v}{\partial t}\big\vert_{\text{dyn}} \Delta p \right\rangle$ | $\left[\frac{1\,Pa}{s}\,s\right]$ | Dynamics |
| $\left\langle \frac{\partial q_v}{\partial t}\big\vert_{\text{diff}} \Delta p \right\rangle$ | $\left[\frac{1\,Pa}{s}\,s\right]$ | Diffusion scheme |
| $\left\langle \frac{\partial q_v}{\partial t}\big\vert_{\text{conv}} \Delta p \right\rangle$ | $\left[\frac{1\,Pa}{s}\,s\right]$ | Convection scheme |
| $\left\langle \frac{\partial q_v}{\partial t}\big\vert_{\text{cloud}} \Delta p \right\rangle$ | $\left[\frac{1\,Pa}{s}\,s\right]$ | Cloud scheme |
| $\left\langle \frac{\partial q_{li}}{\partial t}\big\vert_{\text{para}} \Delta p \right\rangle$ | $\left[\frac{1\,Pa}{s}\,s\right]$ | Conversion to liquid/frozen water (due to entire parametrization) |
| $\left\langle \frac{\partial q_l}{\partial t}\big\vert_{\text{diff}} \Delta p \right\rangle$ | $\left[\frac{1\,Pa}{s}\,s\right]$ | Diffusion scheme |
| $\left\langle \frac{\partial q_i}{\partial t}\big\vert_{\text{diff}} \Delta p \right\rangle$ | $\left[\frac{1\,Pa}{s}\,s\right]$ | Diffusion scheme |
| **Name** | **Unit** | **Accumulated fluxes due to** |
| $\langle F^T_{\text{conv}} \rangle$ | $\left[\frac{K\,kg}{m^2 s}\,s\right]$ | Turbulence (convection scheme) |
| $\langle F^{q_v}_{\text{conv}} \rangle$ | $\left[\frac{kg}{m^2 s}\,s\right]$ | Turbulence (convection scheme) |
| $\langle F^{q_{li}}_{\text{conv}} \rangle$ | $\left[\frac{kg}{m^2 s}\,s\right]$ | Turbulence (convection scheme) |
| $\langle F^r_{\text{conv}} \rangle$ | $\left[\frac{kg}{m^2 s}\,s\right]$ | Liquid convective precipitation |
| $\langle F^s_{\text{conv}} \rangle$ | $\left[\frac{kg}{m^2 s}\,s\right]$ | Frozen convective precipitation |
| $\langle F^r_{\text{cloud}} \rangle$ | $\left[\frac{kg}{m^2 s}\,s\right]$ | Liquid large scale precipitation |
| $\langle F^s_{\text{cloud}} \rangle$ | $\left[\frac{kg}{m^2 s}\,s\right]$ | Frozen large scale precipitation |

model run. These fields are however not sufficient for the present analysis.

Table 2 lists the additional fields stored within the present experiment. Accumulated weighted tendencies are denoted as $\left\langle \frac{\partial X}{\partial t}\big\vert_y \Delta p \right\rangle$, accumulated fluxes as $\langle F^X_y \rangle$. The symbol $X$ indicates the variable involved (temperature $T$, specific humidity $q_v$, liquid cloudwater $q_l$, frozen cloudwater $q_i$, combined liquid/frozen cloudwater $q_{li}$, liquid precipitation $r$ and frozen precipitation $s$), the subscript $y$ the governing process (convection, diffusion, cloud scheme). The operator $\langle\rangle$ is defined as:

$$\langle AB \rangle = \int_{t_0}^{t} AB\,\mathrm{d}t. \tag{31}$$

It is a shorthand notation for the time integral from the initial time $t_0$ of the forecast until the time $t$ for which the accumulated field is eventually archived. The integrand is a product of all time-dependent functions $A$, $B$ involved. Note that the result $\langle AB \rangle$ remains to be a function of the upper limit $t$ of the integration.

Table 2 contains, in addition to the tendencies of $T$ and $q_v$, tendencies of $q_l$, $q_i$ and $q_{li}$ which are required in the calculation of the diffusive contribution to both $w$ and $f$ (see Section A.2). All fields of Tables 1 and 2 were stored every 24 h. They represent the data basis for this study.

Mean fields for the period from time $t_1$ to time $t_2$ can now be calculated from the accumulated fields. For weighted apparent tendencies this reads for example:

$$\frac{\partial T}{\partial t}\bigg|_{\text{conv}} \Delta p = \frac{\left\langle \frac{\partial T}{\partial t}\big|_{\text{conv}} \Delta p \right\rangle (t_2) - \left\langle \frac{\partial T}{\partial t}\big|_{\text{conv}} \Delta p \right\rangle (t_1)}{t_2 - t_1}. \tag{32}$$

In the same way mean fluxes are calculated, for example:

$$F^T_{\text{conv}} = \frac{\left\langle F^T_{\text{conv}} \right\rangle (t_2) - \left\langle F^T_{\text{conv}} \right\rangle (t_1)}{t_2 - t_1}. \tag{33}$$

Experiments with various averaging periods were carried out. Figure 16 shows the annual cycle of the conversion rates for monthly averages (i.e. $t_2 - t_1 = 1$ month), Fig. 17 for daily averages ($t_2 - t_1 = 1$ d). Figures 16 and 17 reveal that the annual average is practically the same for these very different averaging intervals. Concerning the equivalent comparison of the generation rate (Fig. 18) the coincidence is less perfect.

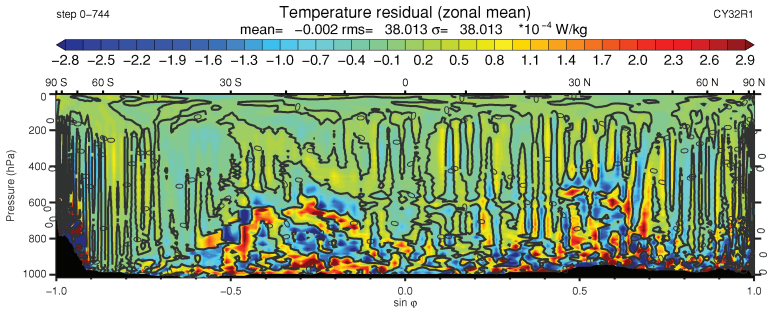


*Fig. 4.* Zonal mean of the residual of eq. (18) for the first forecast month.

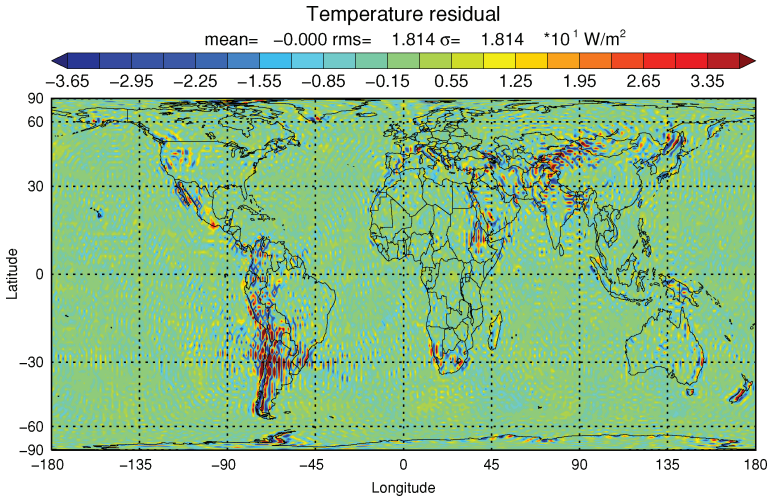


*Fig. 5.* Vertical integral of the residual of eq. (18) for the first forecast month.

Nevertheless it was decided to accept the monthly mean as the standard average.

## 6. Consistency checks

Two different consistency checks were applied on the data from the special model run. First the residuals of eqs (18) and (19) were examined. Second the surface fluxes of $w$ and $f$ from eq. (28) were compared with the routinely stored surface fluxes (Table 1). Both consistency checks were carried out for the first month of the 1-yr climate run (i.e. for 'August')

### 6.1. *Residuals of the forecast equations*

The monthly mean gridscale tendencies of temperature and specific humidity on the left of eqs (18) and (19) are calculated from the routinely stored fields of $\overline{T}$ and $\overline{q}_v$ (Table 1). The appropriate apparent tendencies on the right-hand side of eqs (18) and (19) are individually very large compared with the gridscale tendencies. They were obtained from a 1 month model run. In this way the left- and the right-hand side of eqs (18) and (19) were independently specified. The difference between both sides is called here the residual of the forecast eqs (18) and (19).

Since the residual should be zero at every single time step it is possible in this special case to exchange time and mass integration. This test was therefore not made in the mass-weighted archiving mode but in the regular ECMWF mode.

For the specific humidity (eq. 19, no figure shown) the rms-value of the residual is three orders of magnitude smaller than the corresponding rms-value of the local tendency. The global mass mean of the residual is five orders of magnitude smaller than the mean of the local tendency. Considering the complexity of the IFS these figures are considered as satisfyingly small.

For the temperature (eq. 18, Figs. 4 and 5) the results are less satisfactory. The global mass mean of the residual is $-1.55 \times 10^{-7}$ W kg$^{-1}$, compared to the mean of the temperature tendency of $-6.70 \times 10^{-5}$ W kg$^{-1}$, corresponding to a linear mean residual of 0.2%; this appears as acceptable. However, the rms-value of the residual is twice that of the tendency (rms of residual $3.80 \times 10^{-3}$ W kg$^{-1}$, rms of tendency $1.78 \times 10^{-3}$ W kg$^{-1}$).

The main reason for this strong imbalance seems to be the semi-implicit solution technique applied in the local temperature forecast equation. The purpose of this technique is to filter fast gravity waves; these are generated predominantly in

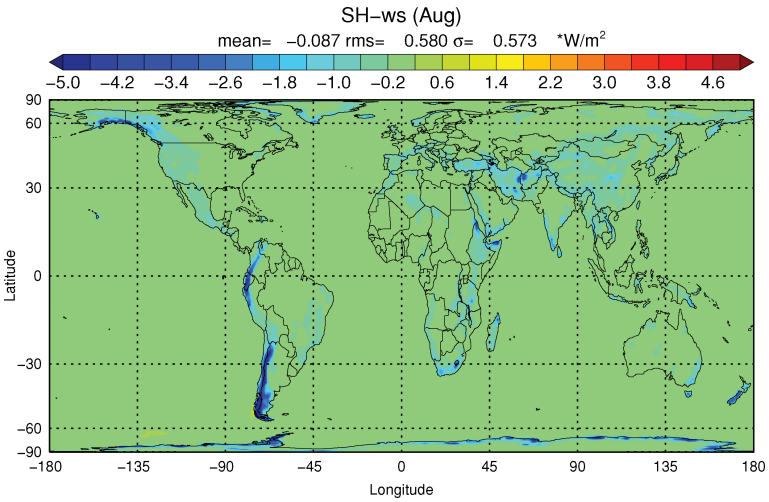


*Fig. 6.* Difference of routinely stored surface sensible heat flux and surface sensible heat flux calculated from eq. (28).

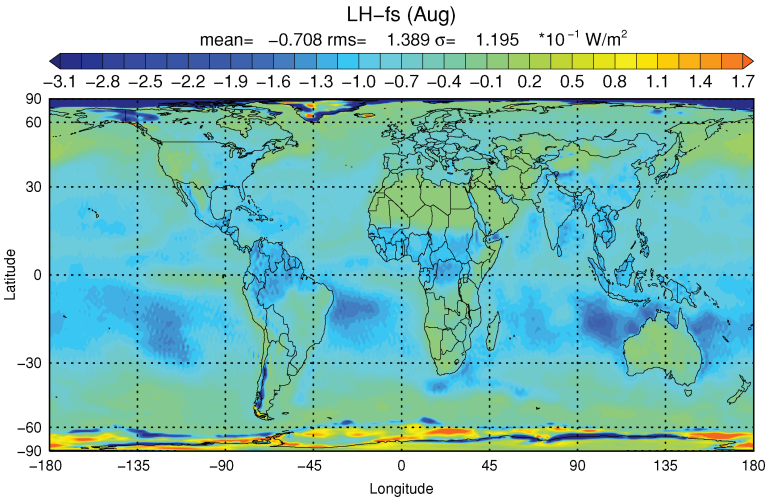


*Fig. 7.* Difference of routinely stored surface latent heat flux and surface latent heat flux calculated from eq. (28).

mountainous terrain. This explains why the residual discrepancy of the temperature forecast equation found in Fig. 5 is most pronounced over the Andes and the Himalayas.

The semi-implicit effect cannot be extracted for specific gridpoints; further, it cannot be split into a gridscale and a subgridscale fraction. For these reasons, the residual was considered as additional apparent temperature tendency generated by the gridscale dynamics and consequently lumped into $\partial T/\partial t|_{\mathrm{dyn}}$.

### 6.2. *Residuals of the surface fluxes*

The consistency of the turbulent fluxes calculated from eq. (28) is tested by comparing them with the operationally stored surface fluxes of sensible and latent heat from the surface parametrization. Figures 6 and 7 show the difference between the operationally stored surface fluxes and the calculated surface fluxes $w$ and $f$, respectively. The global rms-mean of the difference is about 2% of the parametrized flux in the case of $w$ and about 0.1% in the case of $f$. The strongest differences in Fig. 6, typically of the order $5\,\mathrm{W\,m^{-2}}$, are found in a few regions limited to high orography. Concerning the negative anomalies over the subtropical southern oceans in Fig. 7 note that these discrepancies are typically below $0.3\,\mathrm{W\,m^{-2}}$. For these reasons the overall imbalance in Figs. 6 and 7 can be considered satisfyingly small.

## 7. Results

The local gridscale conversion rate $-\overline{\alpha}\,\overline{\omega}$, contained in the budget equation of temperature, was calculated at every time step in the model run and stored as accumulated mass-weighted tendency. The local subgridscale conversion rate $-\overline{\alpha'\omega'}$ was calculated from eq. (9) using the fluxes $w$ and $f$. Also, the gridscale efficiency factor $\overline{N}$ and the response $\overline{R}$ of the atmosphere to heating (i.e. both the gridscale and subgridscale components

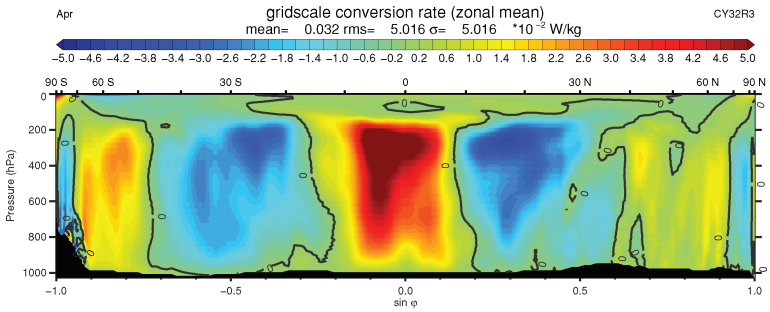


*Fig. 8.* Zonal mean of the local gridscale conversion rate $-\overline{\alpha}\,\overline{\omega}$, valid for the month April of the climate run.

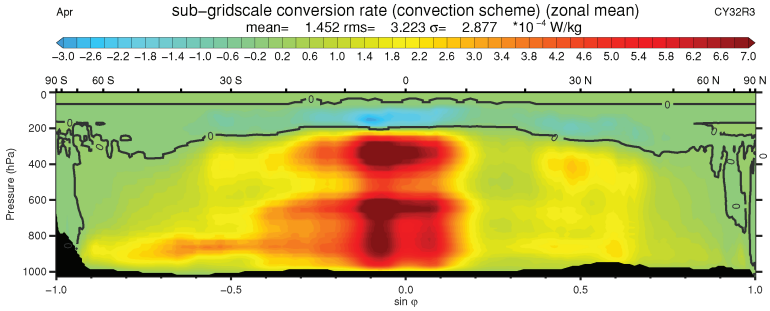


*Fig. 9.* Zonal mean of the local subgridscale conversion rate $-\overline{\alpha'\omega'}$, calculated from fluxes $w$ and $f$ extracted exclusively from the convection scheme. Valid for the month April of the climate run.

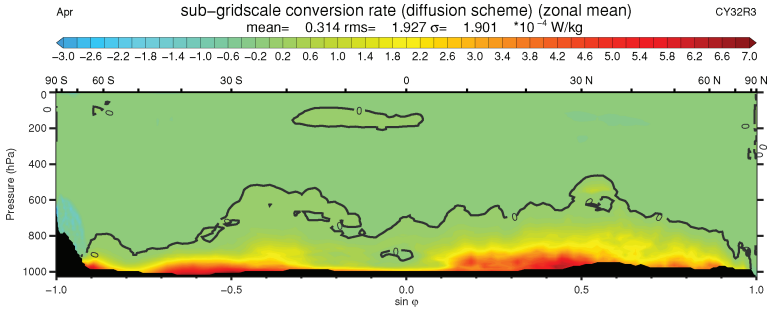


*Fig. 10.* Like Fig. 9, but extracted exclusively from the diffusion scheme.

$\overline{R}^{\text{grid}}$, $\overline{R}^{\text{sub}}$) were calculated. With these fields the conversion rate and the generation rate of the Lorenz cycle, both in its gridscale and subgridscale components, were estimated. The global patterns of these quantities will be discussed first, followed by the corresponding global means.

### 7.1. *Global patterns of the local conversion rates*

Figure 8 displays, for one selected month (April) of the 1-yr climate run, the zonal mean global distribution of the local gridscale conversion rate $-\overline{\alpha}\,\overline{\omega}$. This quantity is a strong component of the sensible heat budget of the atmosphere (e.g. HH-I or Hamelbeck et al., 2001). The global rms-value of the corresponding subgridscale quantity in Fig. 9, the buoyancy flux $-\overline{\alpha'\omega'}$, is typically two orders of magnitude smaller. Figure 9 has been calculated with data exclusively from the convection scheme.

The contribution of small scale turbulence to the buoyancy flux, parametrized by the diffusion scheme of the IFS, is plotted in Fig. 10 for the same month. The global mean, both linear and rms, is considerably smaller than the deep convection component of Fig. 9. Figure 10 shows that the scheme concentrates the diffusive component of $-\overline{\alpha'\omega'}$ to the planetary boundary layer (PBL).

Thus the full buoyancy flux, that is, the sum of Figs. 9 and 10 (see Fig. 13b), is almost identical to Fig. 9. It is predominantly deep organized convection, maximum in the tropical atmosphere, that controls the conversion from subgridscale available potential energy into subgridscale kinetic energy. This is an important result. It implies that the turbulent processes in the PBL control just a small fraction of this conversion, in naive agreement with the limited geometrical extension of the PBL.

The gridscale conversion rate, that is, the linear global mean of Fig. 8, is about $3.2 \times 10^{-4}\,\mathrm{W\,kg^{-1}}$; the subgridscale conversion rate, that is, the linear global mean of Fig. 13b, is $1.8 \times 10^{-4}\,\mathrm{W\,kg^{-1}}$. This shows that both gridscale and subgridscale processes contribute about equally to the global energy conversion rate. However, the rms-values of both global patterns are completely different: $502 \times 10^{-4}\,\mathrm{W\,kg^{-1}}$ in Fig. 8 and

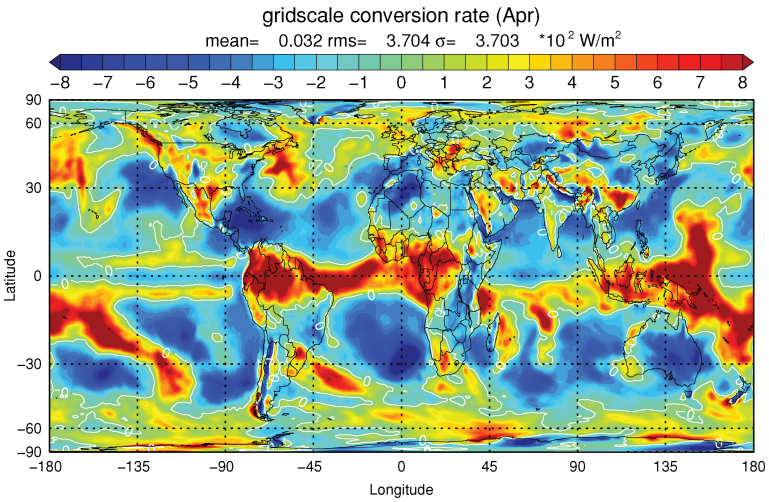


*Fig. 11.* Vertical mean of the local gridscale conversion rate $-\overline{\alpha}\,\overline{\omega}$, valid for the month April. Same as Fig. 8 but vertical integral instead of zonal mean.

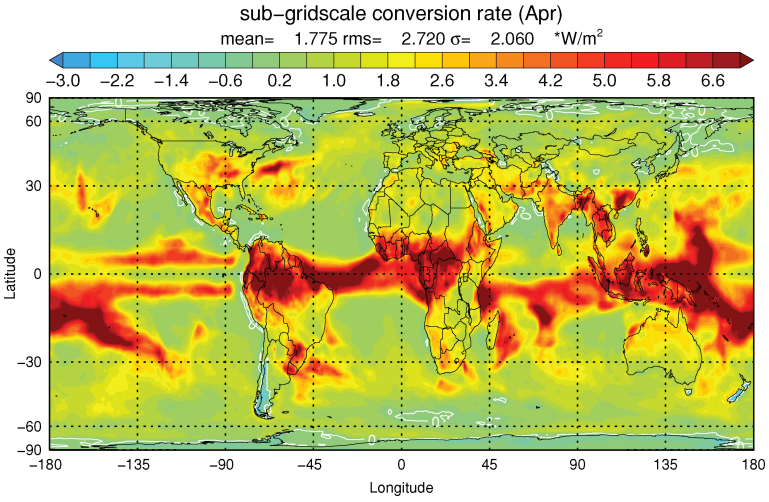


*Fig. 12.* Vertical mean of the local subgridscale conversion rate $-\overline{\alpha'\omega'}$, calculated from fluxes $w$ and $f$. Valid for the month April. Same as Fig. 11 but for buoyancy flux instead of $-\overline{\alpha}\,\overline{\omega}$. White isolines: Zero.

$3.8 \times 10^{-4}\,\mathrm{W\,kg^{-1}}$ in Fig. 13b. It shows that the gridscale conversion rate is the residual of very large values of the adiabatic term with opposite sign which almost exactly compensate each other. For the subgridscale conversion rate this is quite different. The rms-value of Fig. 13b is of about same magnitude as the linear global mean; this implies that the individual field value of the buoyancy flux is representative for the subgridscale conversion rate.

The geographical distribution of the vertical integrals of these fields are shown in Figs. 11 and 12. Both gridscale and subgridscale local conversion rates show distinct maxima in the ITCZ. Again it should be stressed that the global mean of both fields is of comparable size, while the fields are very different. The local gridscale conversion rate is much bigger in magnitude than the local subgridscale conversion rate; however, positive and negative contributions to the global mean almost cancel each other. In contrast the local subgridscale conversion rate is nearly everywhere positive around the globe which yields a comparable mean for much smaller individual values.

The conspicuous correlation of positive areas of $-\overline{\alpha}\,\overline{\omega}$ (Fig. 11) with maxima of $-\overline{\alpha'\omega'}$ (Fig. 12) in the tropics deserves a comment. Positive values of the gridscale adiabatic term are due to upward $\overline{\omega}$ which tends to support convection and thus should be correlated with upward buoyancy flux. However, over areas with downward $\overline{\omega}$ (primarily over the subtropical oceans and also in the extratropics) the buoyancy flux, while weaker, is yet upward directed. Regional examples include the equatorial band of weak but positive buoyancy flux in the Pacific and Indian Oceans or the areas with downward $\overline{\omega}$ and positive buoyancy flux over the Gulf Stream and the Kuroshio regions.

The reason for the buoyancy flux to be directed upward is that the subgridscale vertical velocity is positively correlated with density fluctuations 'on the local scale' since warm air parcels tend to rise and cold air parcels tend to sink. In contrast, $\overline{\alpha}$ is only weakly correlated with $\overline{\omega}$ 'on the global scale' since $\overline{\alpha}$ is always positive. Further examples for the missing coupling between $-\overline{\alpha}\,\overline{\omega}$ and the buoyancy flux are the various strong upward $\overline{\omega}$ maxima in the high latitudes (Central Siberia, coast

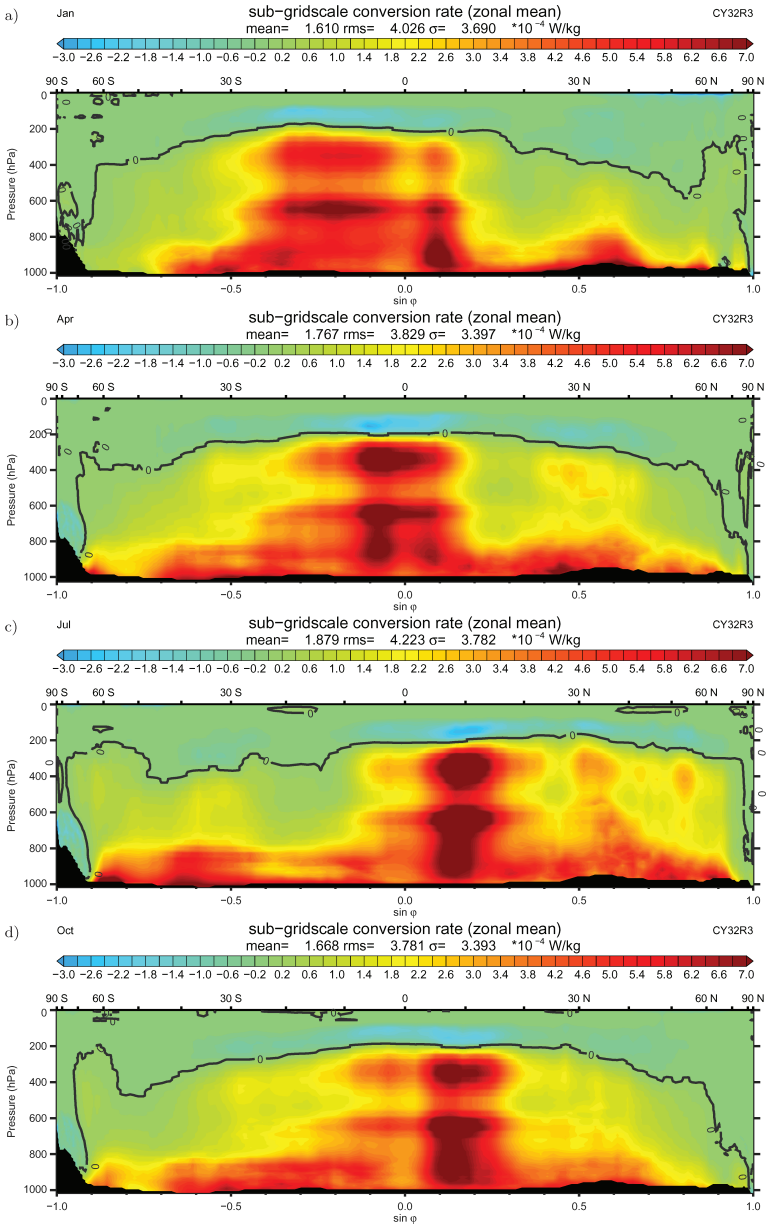


*Fig. 13.* Zonal mean of the buoyancy flux (i.e. the local subgridscale conversion rate $-\overline{\alpha'\omega'}$), calculated from fluxes $w$ and $f$. Valid for the months January, April, July and October of the climate run. Second individual plot (April) equal to sum of Figs. 9, 10.

of Antarctica); these are not at all correlated with any buoyancy flux maximum.

The next step is to discuss the global distribution of the local subgridscale conversion rate. Its seasonal variations are presented in Fig. 13. In this plot the zonal mean of the buoyancy flux is shown for the central month of each season. The figure shows, throughout the global atmosphere and throughout the year, the general upward directed buoyancy flux. One of the three requirements of a rational, well posed, and physically reasonable, parametrization scheme, postulated by Arakawa (2004), is that the parametrization 'should be based on the concept of buoyancy'. According to Arakawa, 'this is a physically reasonable requirement since cumulus convection is buoyant convection, which recognizes its environment primarily through the buoyancy force'. Fig. 13 demonstrates that this requirement has indeed been fulfilled by the present IFS run. The buoyancy flux, implicitly contained in the model forecast run, is maximum throughout the year in the ITCZ. It reaches up to the tropopause which throughout the atmosphere is recognizable as the zero line of $-\overline{\alpha'\omega'}$.

The large layer with weak negative buoyancy flux in the tropical upper troposphere in Fig. 13 is presumably due to convective overshooting. This interpretation is consistent with the similar layer of downward sensible heat flux already found in Fig. 2.

The buoyancy flux is at its maximum in northern summer, when convection over the land areas of the northern hemisphere

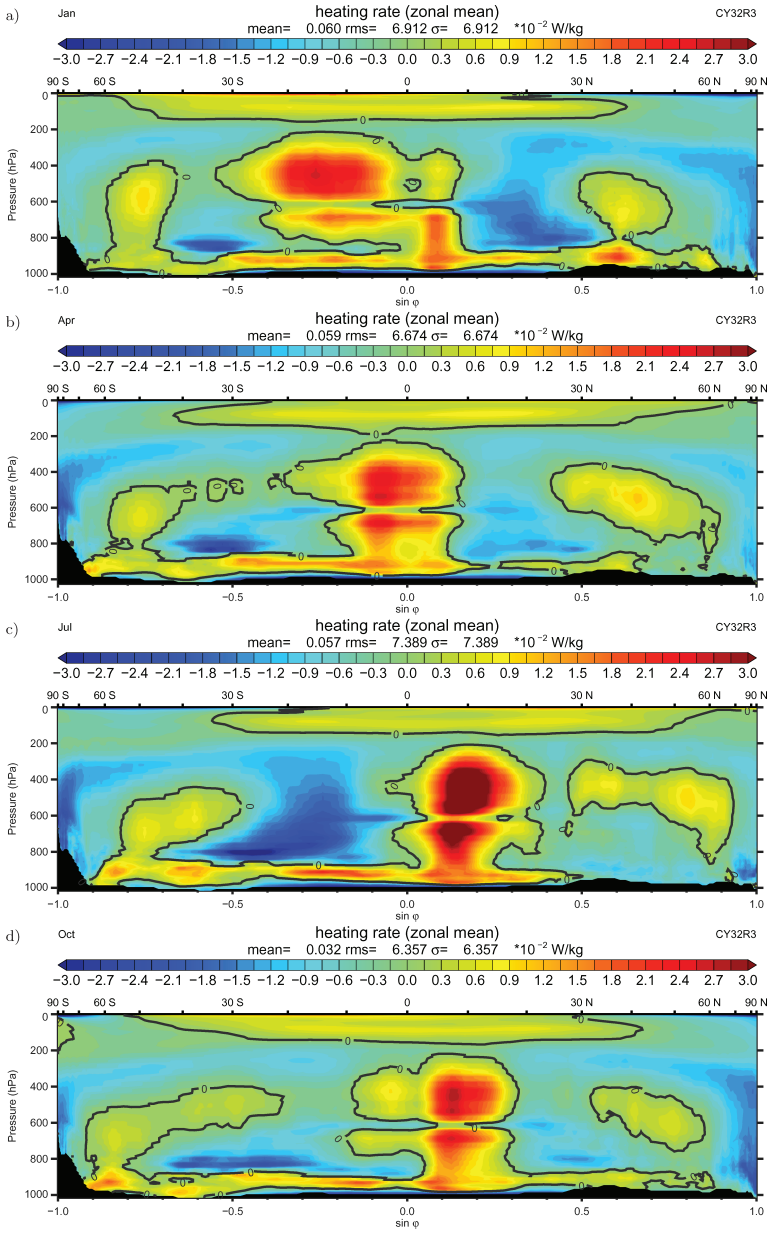


*Fig. 14.* Zonal mean of $\overline{R}$. Valid for the months January, April, July and October of the climate run.

peaks. A corresponding peak on the southern hemisphere does not exist due to the dominating influence of the ocean area.

### *7.2. Global patterns of the local generation rates*

In order to estimate the generation rate $G^{\text{grid}}$ the global distribution of $\overline{R}$ is needed. This quantity, introduced as the 'response' in HH-II, has been defined in eq. (11). The zonal mean of the gridscale response $\overline{R}$, as extracted from the IFS, is plotted in Fig. 14.

This quantity was originally evaluated by Hantel and Baader (1978); their data set (adopted from Oort and Rasmusson, 1971) was limited to coarse gridscale data 1958–1963 of the northern hemisphere (see also fig. 9.10 in Gill, 1982). The same quantity was evaluated for the seasons 1979-1989 with ECMWF data (see pp. 132, 136, 140, 144 of Hoskins et al., 1989) and again by Fortelius (1995).

Figure 14 is in quite good agreement with these earlier evaluations. For example, the global field of $\overline{R}$ reproduces the climatic zones: Condensational heating dominates in the ITCZ and in mid-latitude storm tracks; radiational cooling dominates in the cloud free latitudes of the subtropics and over the polar caps. Specific details, beyond the scope of this study, are visible in the field of $\overline{R}$ in its annual course. For example, the positive area of $\overline{R}$ around 600 hPa in the extratropics is well separated from the boundary layer; it is caused by the

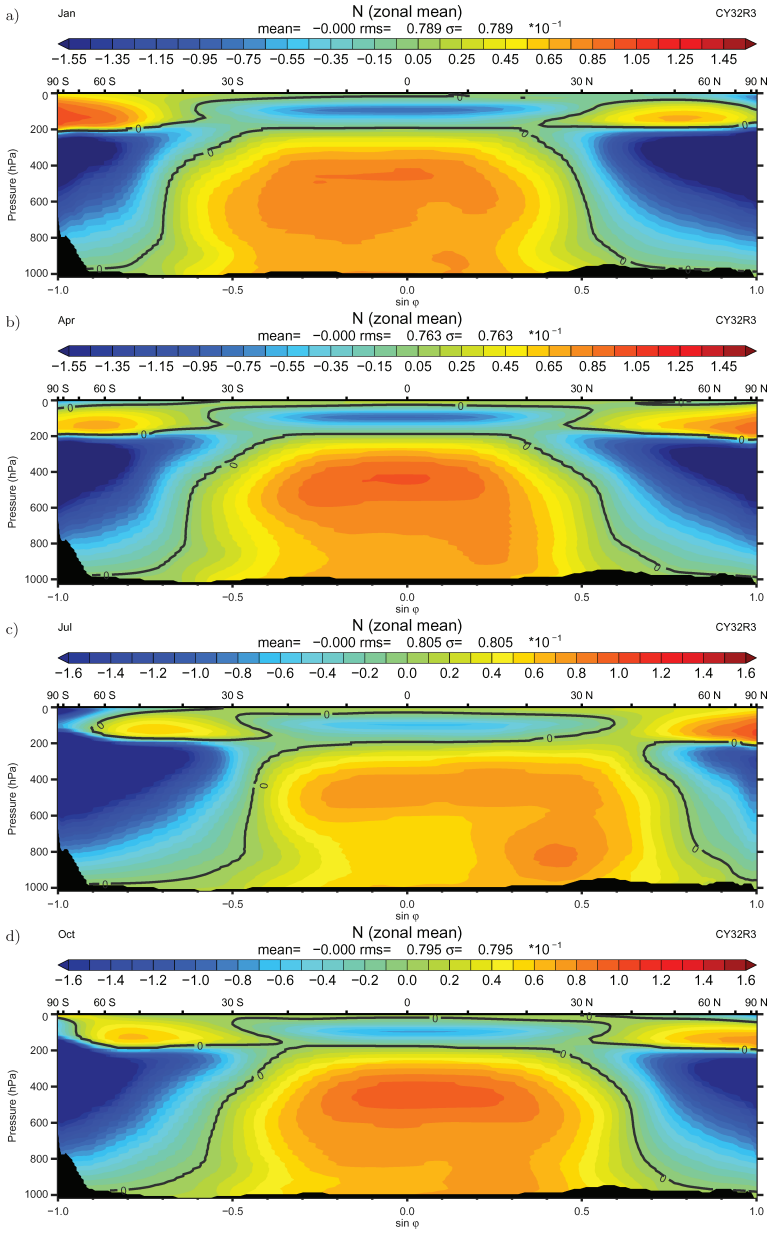


*Fig. 15.* Zonal mean of the efficiency factor $\overline{N}$. Valid for the months January, April, July and October of the climate run.

precipitation generating processes in these latitudes. Another example is the boundary layer heating as well as the stratospheric layer heating.

The innovative aspect in Fig. 14 is however the fact that the subgridscale component has now become accessible and is fully included in $\overline{R}$. For example, Hantel and Baader (1978) were forced to lump the 'subsynoptic term', as they called it, into the quantity $Q$, because they had no possibility to estimate $\overline{R}^{\text{sub}}$. The subgridscale contribution to the present $\overline{R}$ is by no means negligible; it constitutes the second part of $\overline{R}$ according to eq. (11). The structure of the global field of $\overline{R}^{\text{sub}}$ (not shown) is dominated by the vertical divergence of the turbulent sensible heat flux; the buoyancy flux, the second part of $\overline{R}^{\text{sub}}$, is practically not visible. However, the global mean of the turbulent sensible heat flux divergence is zero, since the turbulent sensible heat flux vanishes at the surface and at top of the atmosphere (note: the molecular sensible heat flux, only effective in the skin layer of the surface is not included in eq. 11). Conversely, the buoyancy flux has a global average of 1.73 W m$^{-2}$.

The efficiency factor, defined in eq. (5) and indispensable for estimating the generation rate of available potential energy, has been calculated from the reference pressure; $p_r$ was obtained as the average of $p$ on isentropic surfaces. The corresponding gridscale $\overline{N}$ is plotted in Fig. 15. It is broadly correlated with the pattern of $\overline{R}$. To what extent it is advisable to search for a subgridscale efficiency factor in order to evaluate $\overline{N'Q'}$ and

*Table 3.* Heating-, generation and conversion rates relevant for the global Lorenz energy cycle and discussed in this study, stratified into local and global quantities and gridscale and subgridscale contributions

| | Local | Global |
|---|---|---|
| | Heating rate | |
| Total | $\overline{R}$ | $\{\overline{R}\}$ |
| Gridscale | $\overline{R}^{\mathrm{grid}}$ | $\{\overline{R}^{\mathrm{grid}}\}$ |
| Subgridscale | $\overline{R}^{\mathrm{sub}}$ | $\{\overline{R}^{\mathrm{sub}}\}$ |
| | Generation rate | |
| Total | $\overline{N}\,\overline{R}$ | $G = \{\overline{N}\,\overline{R}\}$ |
| Gridscale | $\overline{N}\,\overline{R}$ | $G^{\mathrm{grid}} = \{\overline{N}\,\overline{R}\}$ |
| Subgridscale | $\overline{N'R'}$ | $G^{\mathrm{sub}} = \{\overline{N'R'}\}$ |
| | Conversion rate | |
| Total | $-\overline{\alpha}\,\overline{\omega}$ | $C = \{-\overline{\alpha}\,\overline{\omega}\}$ |
| Gridscale | $-\overline{\alpha}\,\overline{\omega}$ | $C^{\mathrm{grid}} = \{-\overline{\alpha}\,\overline{\omega}\}$ |
| Subgridscale | $-\overline{\alpha'\omega'}$ | $C^{\mathrm{sub}} = \{-\overline{\alpha'\omega'}\}$ |

its corresponding global integral $G^{\mathrm{sub}}$ may be left here for later consideration.

### 7.3. A new estimate of the Lorenz global energy cycle

The local and global quantities discussed in this study, which are required for a state-of-the-art estimate of the classical Lorenz energy cycle, complete with the subgridscale components, are listed in Table 3. All quantities in this table have been explicitly evaluated from the results of the present 1-yr IFS run in climate mode except the subgridscale generation rate $\overline{N'R'}$ and its corresponding global average $G^{\mathrm{sub}}$. The global patterns of the column in Table 3 referred to as 'local' have been discussed before.

The next step is to discuss the 'global' quantities which are obtained from the corresponding local quantities through global mass integration. These global quantities represent the components of a new estimate of the Lorenz energy cycle.

Time-series of the monthly global mean values of gridscale and subgridscale conversion rates $\{-\overline{\alpha}\,\overline{\omega}\}$, $\left\{-\overline{\alpha'\omega'}\right\}$ are shown in Fig. 16. Both conversion rates show little time variation throughout the year. The slightly smaller subgridscale conversion rate in southern summer is in agreement with the smaller convective activity during this season; it is caused by the different land–sea distribution on the southern as opposed to the northern hemisphere.

The conversion rates $C^{\mathrm{grid}}$ and $C^{\mathrm{sub}}$ have been calculated as annual mean from the twelve monthly averages. The result is:

$$C^{\mathrm{grid}} = (3.39 \pm 0.12)\ \mathrm{W\,m^{-2}}; \tag{34}$$

$$C^{\mathrm{sub}} = (1.73 \pm 0.10)\ \mathrm{W\,m^{-2}}; \tag{35}$$

$$C = (5.12 \pm 0.22)\ \mathrm{W\,m^{-2}}. \tag{36}$$

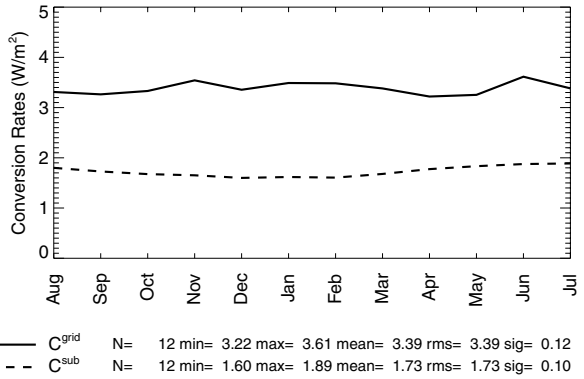


*Fig. 16.* Time-series of monthly mean gridscale and subgridscale conversion rates calculated from the 1-yr climate forecast.

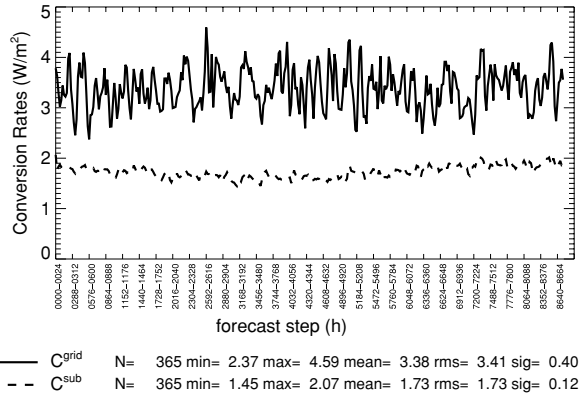


*Fig. 17.* Time-series of 24 hourly gridscale and subgridscale conversion rates calculated from the 1-yr climate forecast.

The standard deviation of the monthly values in Fig. 16 has been taken as the error estimate. These figures represent the central result of this study.

How can it be excluded that there is no systematic positive error in the computed buoyancy flux? From formula (9) it is clear that such error would be caused by a negative systematic error of $w$ and/or $f$, in other words, by a systematic error of the parametrization. It appears impossible to exclude this error.

In order to study the role of the short synoptic fluctuations global averages on a daily basis have additionally been calculated. The results, corresponding to the monthly time-series of Fig. 16, are plotted as daily time-series in Fig. 17. The daily fluctuations of $C^{\mathrm{grid}}$ are three to four times larger than the monthly fluctuations as shown by the values of $\sigma$. However, the annual mean is practically the same in Figs. 16 and 17.

This coincidence is no independent test since the monthly data have been gained by straight time integration of the daily data. The coincidence is predominantly a further consistency check of the present numerical experiment. However, it also adds additional daily variance. The first main message from Figs. 16 and 17 is that the conversion rate is relatively steady throughout

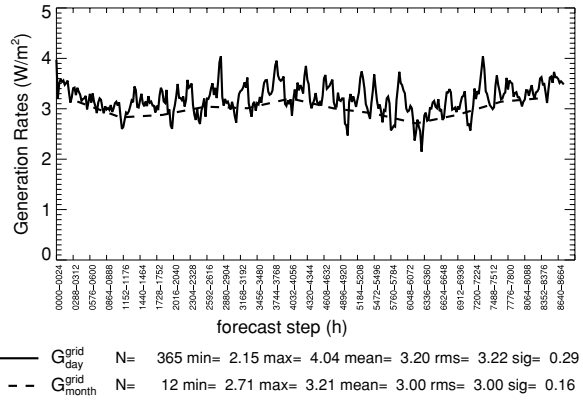


*Fig. 18.* Time-series of 24 hourly (full curve) and monthly (dashed curve) gridscale generation rate, calculated from the 1-yr climate forecast.

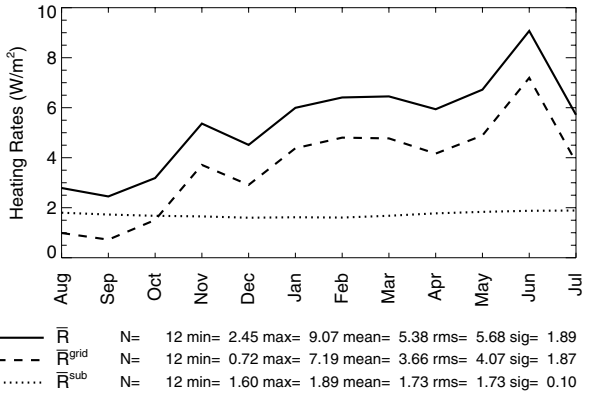


*Fig. 19.* Time-series of monthly mean gridscale and subgridscale heating rates calculated from the 1-yr climate forecast.

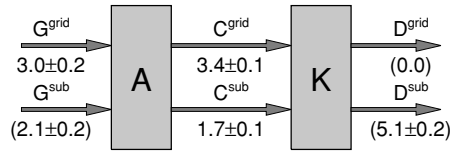


*Fig. 20.* Global energy cycle extracted from a 1-yr climate forecast of IFS. Reservoirs of available potential and kinetic energy $A$ and $K$. Traditional gridscale conversion rates $G^{\mathrm{grid}}$, $C^{\mathrm{grid}}$ and $D^{\mathrm{grid}}$. Subgridscale conversion rates $G^{\mathrm{sub}}$, $C^{\mathrm{sub}}$ and $D^{\mathrm{sub}}$. Values in parentheses inferred for stationary reservoirs $A$ and $K$.

the model year; one arbitrary month would already be sufficient to estimate the climate mean of both $C^{\mathrm{grid}}$, $C^{\mathrm{sub}}$. The second main message is the coincidence with the preliminary results of HH-II (see also Fig. 1). Their estimate ($(4.7 \pm 1.7)$ W m$^{-2}$) coincides, within error margins, with the estimate (36).

Turning now to the gridscale generation rate $G^{\mathrm{grid}}$ a first estimate comes from the monthly averages of both $\overline{N}$ and $\overline{R}$ (Fig. 18, dashed curve). A second estimate is from the daily values of the same quantities (full curve). The corresponding annual means are:

$$G^{\mathrm{grid}}_{\mathrm{month}} = (3.00 \pm 0.16)\ \mathrm{W\,m^{-2}};\quad G^{\mathrm{grid}}_{\mathrm{day}} = (3.20 \pm 0.29)\ \mathrm{W\,m^{-2}}. \tag{37}$$

The errors given are from the monthly variance (the daily variance in case of $G^{\mathrm{grid}}_{\mathrm{day}}$) and thus are mostly due to the annual wave which is an overestimate. Thus the difference between the two estimates of $G^{\mathrm{grid}}$ is presumably significant. The difference is due to the fact that the daily efficiency factor calculated for $G^{\mathrm{grid}}_{\mathrm{day}}$ caused some additional correlation with the local heating rate. This augmentation of $G^{\mathrm{grid}}$ should however not be interpreted as the unavailable subgridscale quantity $G^{\mathrm{sub}}$. Rather, the figure most consistent with the other fluxes of this study appears to be $G^{\mathrm{grid}}_{\mathrm{month}}$; this estimate has been entered in Fig. 20.

Although the subgridscale quantity $G^{\mathrm{sub}}$ is unavailable, because explicit subgridscale data are fundamentally missing, there is an indirect way to estimate $G^{\mathrm{sub}}$, by using the correspondence:

$$G^{\mathrm{grid}} + G^{\mathrm{sub}} = C^{\mathrm{grid}} + C^{\mathrm{sub}} \tag{38}$$

which should prevail in a stationary climate. From eq. (38) together with (36), (37) the indirect estimate of the subgridscale generation rate follows:

$$G^{\mathrm{sub}} = (2.1 \pm 0.2)\ \mathrm{W\,m^{-2}}. \tag{39}$$

This indirect estimate is the best one can presently offer. This is supported by the very small annual time tendency of the reservoirs of both gridscale available potential and kinetic energy (not shown here) which are below 0.1 W m$^{-2}$.

There is a further, partially independent, estimate of the total generation rate in form of $\{\overline{R}\}$. This is shown in Fig. 19. The global mean of $\overline{R}^{\mathrm{grid}}$ undergoes a considerable seasonal fluctuation with an annual mean of 3.66 W m$^{-2}$. In contrast, the global mean of $\overline{R}^{\mathrm{sub}}$, which is identical to the one of the buoyancy flux (eq. 11), is practically constant throughout the year with a global mean of 1.73 W m$^{-2}$.

One important aspect of $\overline{R}$ is that its global mean can be taken as independent estimate of the generation rate $G$ of available potential energy, at least in the climate time mean. The independence is of a principal nature; actually, the estimate is not independent. Since $G$ cannot in practice be determined without reference to the sensible heat budget, which has already been the basis of $\overline{R}$, the values found for $G$ and $\{\overline{R}\}$ are practically related to each other.

From Fig. 19, by using the sum of $\overline{R}^{\mathrm{grid}}$ and $\overline{R}^{\mathrm{sub}}$, it follows:

$$\{\overline{R}\} = (5.38 \pm 1.89)\ \mathrm{W\,m^{-2}}. \tag{40}$$

The high error is due to the sizeable annual fluctuation of the heating rate seen in Fig. 19, and therefore presumably an overestimate.

It is nevertheless both important and satisfying that the estimate (36) for the Lorenz conversion rate $C$ and the estimate (40) for the global heating rate coincide within error margins.

The results discussed are summarized in Fig. 20 which is the equivalent to Fig. 1. It represents Lorenz's global energy cycle, complete with both gridscale and subgridscale components, estimated from the gridscale model output and the parametrization drawn from the IFS run, 1 yr in climate mode. The estimates have been rounded to one decimal. Values in parentheses are the indirectly inferred estimates.

Both block Figs. 1 and 20 are surprisingly similar despite the fact that they are based upon entirely different and independent data sets: The estimate of HH-II upon three selected months of the preliminary ERA data set, the present estimate upon a 1-yr forecast with the latest version of IFS. Yet the figures differ only within error margins. Therefore, this study supports the conclusion of HH-II that the subgridscale processes play an important role in Lorenz's global energy cycle and must be included in its evaluation.

In addition to the presented run with CY32R3 a run with CY32R1 was carried out. The results for the global estimates were the same within error margins (not demonstrated here in detail). This shows the relative insensitivity of the present estimates to the change in physical parametrization that has been implemented in the transformation from CY32R1 to CY32R3.

These results are further supported by a series of high-resolution T511 (40 km) short-range forecasts distributed over the year, where the forecasts remains very close to the analysis (not reproduced here).

## 8. Conclusions

This study has tried to estimate the convective component of the global Lorenz energy cycle with the complete data set available from a 1-yr run in climate mode of the ECMWF model (CY32R3). This setting offered a basic data set with unprecedented completeness and accuracy. For the purpose of completing the Lorenz energy cycle the following chain of (both theoretical and practical) tasks had to be carried out and numerically implemented:

(1) The equations of the global energy cycle have been written in a local form that is compatible with the Lorenz theory.

(2) To represent the local equations numerically on the computer requires specification of a grid. The gridscale fixes the space/time scale characteristic for the actual experiment carried out in this study with the IFS.

(3) Discretizing the local equations is equivalent to averaging the Lorenz energy equations over the grid cell. This process is denoted by the overbar operator. It means an average over a space/time cell the size of which is that of the IFS. Averaging non-linear quantities in the equations generates both gridscale and subgridscale terms.

(4) The most prominent non-linear term to be averaged is $-\alpha\omega$ in the temperature equation. Its gridscale component, explicitly included in the IFS, has been $-\overline{\alpha}\,\overline{\omega}$. Its subgridscale (or simply convective) component has been the buoyancy flux $-\overline{\alpha'\omega'}$. Both have been familiarly interpreted as local conversion terms between available potential and kinetic energy.

(5) Likewise the averaged equations involve the local generation of available potential energy, expressed as gridscale component $\overline{N}\,\overline{Q}$ and subgridscale component $\overline{N'Q'}$; here, $N$ is the Lorenz efficiency factor and $Q$ the net heating. Instead of diagnosing $Q$ the response $R$ of the atmosphere to $Q$, expressed through the sensible heat equation, has been used for diagnosing the net heating.

(6) Thus the following gridscale fields were directly extracted from the IFS: $\overline{\alpha}$, $\overline{\omega}$, $\overline{R}^{\mathrm{grid}}$. The gridscale $\overline{N}$ was gained from the mean temperature and pressure fields through global averaging of $p$ on isentropic surfaces.

(7) Further, the following subgridscale fields were indirectly computed from the IFS: The buoyancy flux $-\overline{\alpha'\omega'}$ was gained through determining the sensible and latent heat fluxes $w$ and $f$ and using eq. (9). $\overline{R}^{\mathrm{sub}}$ was gained from $w$ and $-\overline{\alpha'\omega'}$ by using eq. (11). The correlation $\overline{N'Q'}$ could not be estimated.

(8) From these local quantities the corresponding generation and conversion rates $G^{\mathrm{grid}}$, $C^{\mathrm{grid}}$ and $C^{\mathrm{sub}}$ were gained through global mass integration.

(9) $G^{\mathrm{sub}}$ could not be determined. However, since in the climate mean $G$ should be equal to $C$ the subgridscale generation rate was estimated indirectly from $G^{\mathrm{grid}}$, $C^{\mathrm{grid}}$ and $C^{\mathrm{sub}}$.

(10) $D$ could not be determined either, neither $D^{\mathrm{grid}}$ nor $D^{\mathrm{sub}}$. It was assumed that, since dissipation is a molecular process, $D^{\mathrm{grid}}$ needs to be zero. Consequently, the entire dissipation must be subgridscale. Thus $D^{\mathrm{sub}}$ was set equal to the sum $C^{\mathrm{grid}} + C^{\mathrm{sub}}$.

With these steps the goal of independently estimating the key components of the global energy cycle in form of Fig. 20 has been reached. The most important results have been as follows:

(1) The buoyancy flux is directed upward throughout most of the global atmosphere; it is largely controlled by the mechanism of deep convection and thus has its maxima in the tropics. This corroborates the results first reported in HH-II that the buoyancy flux represents the integrand of the new subgridscale conversion rate $C^{\mathrm{sub}}$ from available potential to kinetic energy. $C^{\mathrm{sub}}$ is to be considered as a relevant component of the global energy cycle.

(2) The gridscale conversion rate $C^{\mathrm{grid}}$ from available potential to kinetic energy has come out somewhat larger as the earlier estimates.

(3) The new subgridscale generation rate $G^{\mathrm{sub}}$ of available potential energy could not be independently estimated but was found from balance requirements.

(4) By including the subgridscale components the Lorenz energy cycle from the 1-yr climate run of the IFS has been completely determined and is reproduced in Fig. 20.

(5) According to Fig. 20 the intensity of the global atmospheric circulation is $(5.1 \pm 0.2)$ W m$^{-2}$. This is about twice as intense as all existing earlier estimates have suggested (e.g. Li et al., 2007; Boer and Lambert, 2008).

The reason that the present results are about twice as big as the estimates of other researchers is that not only the gridscale but also the subgridscale conversion of the global energy cycle has been included. Both conversion rates are similarly relevant.

Concerning the gridscale component, the $C^{\mathrm{grid}} = (3.39 \pm 0.12)\,\mathrm{W\,m^{-2}}$ found above is principally in accord with independent estimates. For example, Boer and Lambert (2008) calculated the conversion rate, averaged over the AMIP2 period 1979–1995, for an ensemble of 12 models; their conversion rate may be called $C^{\mathrm{BL}}$. Specifically for the ECMWF model they obtain $C^{\mathrm{BL}} = 3.1\,\mathrm{W\,m^{-2}}$. Since this conversion rate is based on gridscale data, $C^{\mathrm{BL}}$ does not correspond to $C$ but to $C^{\mathrm{grid}}$. The remaining difference between $C^{\mathrm{BL}}$ and $C^{\mathrm{grid}}$ is due to different data representations (e.g. $p$-surfaces versus $\eta$-surfaces) and to different averaging intervals (17 yr versus 1 yr).

However, the philosophy of this study has been that $C^{BL}$ is not the proper quantity for the global energy cycle because it does not comprise the subgridscale component. In fact, this component belongs to the global energy cycle, not the least because the buoyancy flux is of equal sign practically over the entire global atmosphere. When the subgridscale component becomes included, as in this study, the total conversion rate between available potential and kinetic energy jumps to about $(5.1 \pm 0.2)\,\mathrm{W\,m^{-2}}$.

Given that this study has yielded a new perspective to the Lorenz energy cycle what value would be added if modelers were to implement the subgridscale branch of the energy cycle? The implementation of the subgridscale branch would only be consistent if the budget of turbulent kinetic energy (TKE) is explicitly carried in the model. It goes beyond the scope of this study to discuss whether it is advantageous to include the TKE budget in a model. However, if the TKE budget is included, the subgridscale branch of the energy cycle will be relevant.

## 9. Acknowledgments

Acknowledgment is made for use of ECMWF's computing and archive facilities within this research. Leopold Haimberger was very helpful in discussions about the physics and the numerical details of the entire study. Martin Steinheimer has been funded by DOC [Ph.D. scholarship program]; the financial support of this work, including the publication costs, was generously granted by the Austrian Academy of Sciences.

## 10. Appendix

### A.1. Tendency contributions of the parametrization schemes

The parametrized tendencies ($P_T$ and $P_q$) in the budget eqs (14) and (15) have been split into contributions by the various parametrization schemes in eqs (16) and (17). In turn these tendencies can be split into fractions according to the underlying physical processes. Table 4 lists all these terms.

### A.2. Flux contributions from the diffusion scheme

As pointed out in Sections 4.3 and A.1 the apparent tendencies of the state variables calculated by the individual parametrization schemes can be split into contributions due to turbulent transport, phase changes and in case of temperature also dissipation and gravity wave drag. However, dissipation and gravity wave drag were not stored in the diffusive tendency in this experiment (expressed through an additional subscript $*$, see Table 2). The diffusion scheme also does not generate precipitation (i.e. no phase changes incorporating rain and snow). Hence the tendencies of temperature $T$, specific humidity $q_v$, liquid cloud water $q_l$ and frozen cloud water $q_i$ due to the diffusion scheme read

*Table 4.* Physical processes contributing to the individual parametrization schemes

| Apparent tendency | | Turbulent transport | | Condensation/ sublimation | | Freezing | | Dissipation | | Gravity wave drag |
|---|---|---|---|---|---|---|---|---|---|---|
| $\frac{\partial T}{\partial t}\big\vert_{\mathrm{diff}}$ | = | $\frac{\partial T}{\partial t}\big\vert^{\mathrm{turb}}_{\mathrm{diff}}$ | + | $\frac{\partial T}{\partial t}\big\vert^{v\leftrightarrow lirs}_{\mathrm{diff}}$ | + | $\frac{\partial T}{\partial t}\big\vert^{lr\leftrightarrow is}_{\mathrm{diff}}$ | + | $\frac{\partial T}{\partial t}\big\vert^{diss}_{\mathrm{diff}}$ | + | $\frac{\partial T}{\partial t}\big\vert^{gw}_{\mathrm{diff}}$ |
| $\frac{\partial T}{\partial t}\big\vert_{\mathrm{conv}}$ | = | $\frac{\partial T}{\partial t}\big\vert^{\mathrm{turb}}_{\mathrm{conv}}$ | + | $\frac{\partial T}{\partial t}\big\vert^{v\leftrightarrow lirs}_{\mathrm{conv}}$ | + | $\frac{\partial T}{\partial t}\big\vert^{lr\leftrightarrow is}_{\mathrm{conv}}$ | + | ~~$\frac{\partial T}{\partial t}\big\vert^{diss}_{\mathrm{conv}}$~~ | + | ~~$\frac{\partial T}{\partial t}\big\vert^{gw}_{\mathrm{conv}}$~~ |
| $\frac{\partial T}{\partial t}\big\vert_{\mathrm{cloud}}$ | = | ~~$\frac{\partial T}{\partial t}\big\vert^{\mathrm{turb}}_{\mathrm{cloud}}$~~ | + | $\frac{\partial T}{\partial t}\big\vert^{v\leftrightarrow lirs}_{\mathrm{cloud}}$ | + | $\frac{\partial T}{\partial t}\big\vert^{lr\leftrightarrow is}_{\mathrm{cloud}}$ | + | ~~$\frac{\partial T}{\partial t}\big\vert^{diss}_{\mathrm{cloud}}$~~ | + | ~~$\frac{\partial T}{\partial t}\big\vert^{gw}_{\mathrm{cloud}}$~~ |
| $\frac{\partial q_v}{\partial t}\big\vert_{\mathrm{diff}}$ | = | $\frac{\partial q_v}{\partial t}\big\vert^{\mathrm{turb}}_{\mathrm{diff}}$ | + | $\frac{\partial q_v}{\partial t}\big\vert^{v\leftrightarrow lirs}_{\mathrm{diff}}$ | | | | | | |
| $\frac{\partial q_v}{\partial t}\big\vert_{\mathrm{conv}}$ | = | $\frac{\partial q_v}{\partial t}\big\vert^{\mathrm{turb}}_{\mathrm{conv}}$ | + | $\frac{\partial q_v}{\partial t}\big\vert^{v\leftrightarrow lirs}_{\mathrm{conv}}$ | | | | | | |
| $\frac{\partial q_v}{\partial t}\big\vert_{\mathrm{cloud}}$ | = | ~~$\frac{\partial q_v}{\partial t}\big\vert^{\mathrm{turb}}_{\mathrm{cloud}}$~~ | + | $\frac{\partial q_v}{\partial t}\big\vert^{v\leftrightarrow lirs}_{\mathrm{cloud}}$ | | | | | | |

*Note:* All processes that potentially contribute have been listed; those that are not presently implemented have been crossed out.

(see eqs 20 and 22, Table 4):

$$\left.\frac{\partial T}{\partial t}\right|_{\mathrm{diff},*} = \left.\frac{\partial T}{\partial t}\right|_{\mathrm{diff}}^{\mathrm{turb}} + \left.\frac{\partial T}{\partial t}\right|_{\mathrm{diff}}^{v\leftrightarrow l} + \left.\frac{\partial T}{\partial t}\right|_{\mathrm{diff}}^{v\leftrightarrow i} + \left.\frac{\partial T}{\partial t}\right|_{\mathrm{diff}}^{l\leftrightarrow i} \tag{41}$$

$$\left.\frac{\partial q_v}{\partial t}\right|_{\mathrm{diff}} = \left.\frac{\partial q_v}{\partial t}\right|_{\mathrm{diff}}^{\mathrm{turb}} + \left.\frac{\partial q_v}{\partial t}\right|_{\mathrm{diff}}^{v\leftrightarrow l} + \left.\frac{\partial q_v}{\partial t}\right|_{\mathrm{diff}}^{v\leftrightarrow i} \tag{42}$$

$$\left.\frac{\partial q_l}{\partial t}\right|_{\mathrm{diff}} = \left.\frac{\partial q_l}{\partial t}\right|_{\mathrm{diff}}^{\mathrm{turb}} + \left.\frac{\partial q_l}{\partial t}\right|_{\mathrm{diff}}^{l\leftrightarrow v} + \left.\frac{\partial q_l}{\partial t}\right|_{\mathrm{diff}}^{l\leftrightarrow i} \tag{43}$$

$$\left.\frac{\partial q_i}{\partial t}\right|_{\mathrm{diff}} = \left.\frac{\partial q_i}{\partial t}\right|_{\mathrm{diff}}^{\mathrm{turb}} + \left.\frac{\partial q_i}{\partial t}\right|_{\mathrm{diff}}^{i\leftrightarrow v} + \left.\frac{\partial q_i}{\partial t}\right|_{\mathrm{diff}}^{i\leftrightarrow l} \tag{44}$$

For the phase change fractions the following relations should hold:

$$\left.\frac{\partial q_v}{\partial t}\right|_{\mathrm{diff}}^{v\leftrightarrow l} = -\left.\frac{\partial q_l}{\partial t}\right|_{\mathrm{diff}}^{l\leftrightarrow v} = -\frac{c_p}{L_v}\left.\frac{\partial T}{\partial t}\right|_{\mathrm{diff}}^{v\leftrightarrow l} \tag{45}$$

$$\left.\frac{\partial q_v}{\partial t}\right|_{\mathrm{diff}}^{v\leftrightarrow i} = -\left.\frac{\partial q_i}{\partial t}\right|_{\mathrm{diff}}^{i\leftrightarrow v} = -\frac{c_p}{L_i}\left.\frac{\partial T}{\partial t}\right|_{\mathrm{diff}}^{v\leftrightarrow i} \tag{46}$$

$$\left.\frac{\partial q_l}{\partial t}\right|_{\mathrm{diff}}^{l\leftrightarrow i} = -\left.\frac{\partial q_i}{\partial t}\right|_{\mathrm{diff}}^{i\leftrightarrow l} \tag{47}$$

$$\left.\frac{\partial T}{\partial t}\right|_{\mathrm{diff}}^{l\leftrightarrow i} = -\frac{(L_i - L_v)}{c_p}\left.\frac{\partial q_l}{\partial t}\right|_{\mathrm{diff}}^{l\leftrightarrow i} = \frac{(L_i - L_v)}{c_p}\left.\frac{\partial q_i}{\partial t}\right|_{\mathrm{diff}}^{i\leftrightarrow l}. \tag{48}$$

Subtracting $L_v/c_p \times$ (43) and $L_i/c_p \times$ (44) from (41) and observing relations (45)–(48) yields:

$$\begin{aligned}
&\left.\frac{\partial T}{\partial t}\right|_{\mathrm{diff},*} - \frac{L_v}{c_p}\left.\frac{\partial q_l}{\partial t}\right|_{\mathrm{diff}} - \frac{L_i}{c_p}\left.\frac{\partial q_i}{\partial t}\right|_{\mathrm{diff}} \\
&\quad = \left.\frac{\partial T}{\partial t}\right|_{\mathrm{diff}}^{\mathrm{turb}} - \frac{L_v}{c_p}\left.\frac{\partial q_l}{\partial t}\right|_{\mathrm{diff}}^{\mathrm{turb}} - \frac{L_i}{c_p}\left.\frac{\partial q_i}{\partial t}\right|_{\mathrm{diff}}^{\mathrm{turb}} \\
&\quad + \left.\frac{\partial T}{\partial t}\right|_{\mathrm{diff}}^{l\leftrightarrow i} - \frac{L_v}{c_p}\left.\frac{\partial q_l}{\partial t}\right|_{\mathrm{diff}}^{l\leftrightarrow i} - \frac{L_i}{c_p}\left.\frac{\partial q_i}{\partial t}\right|_{\mathrm{diff}}^{i\leftrightarrow l} \\
&\quad = \left.\frac{\partial T}{\partial t}\right|_{\mathrm{diff}}^{\mathrm{turb}} - \frac{L_v}{c_p}\left.\frac{\partial q_l}{\partial t}\right|_{\mathrm{diff}}^{\mathrm{turb}} - \frac{L_i}{c_p}\left.\frac{\partial q_i}{\partial t}\right|_{\mathrm{diff}}^{\mathrm{turb}} \\
&\quad + \left.\frac{\partial T}{\partial t}\right|_{\mathrm{diff}}^{l\leftrightarrow i} - \frac{L_v}{c_p}\left.\frac{\partial q_l}{\partial t}\right|_{\mathrm{diff}}^{l\leftrightarrow i} + \frac{L_i}{c_p}\left.\frac{\partial q_l}{\partial t}\right|_{\mathrm{diff}}^{l\leftrightarrow i} \\
&\quad = \left.\frac{\partial T}{\partial t}\right|_{\mathrm{diff}}^{\mathrm{turb}} - \frac{L_v}{c_p}\left.\frac{\partial q_l}{\partial t}\right|_{\mathrm{diff}}^{\mathrm{turb}} - \frac{L_i}{c_p}\left.\frac{\partial q_i}{\partial t}\right|_{\mathrm{diff}}^{\mathrm{turb}} \\
&\quad + \left.\frac{\partial T}{\partial t}\right|_{\mathrm{diff}}^{l\leftrightarrow i} + \left(\frac{L_i}{c_p} - \frac{L_v}{c_p}\right)\left.\frac{\partial q_l}{\partial t}\right|_{\mathrm{diff}}^{l\leftrightarrow i} \\
&\quad = \left.\frac{\partial T}{\partial t}\right|_{\mathrm{diff}}^{\mathrm{turb}} - \frac{L_v}{c_p}\left.\frac{\partial q_l}{\partial t}\right|_{\mathrm{diff}}^{\mathrm{turb}} - \frac{L_i}{c_p}\left.\frac{\partial q_i}{\partial t}\right|_{\mathrm{diff}}^{\mathrm{turb}}.
\end{aligned} \tag{49}$$

The tendencies on the left-hand side are available from our experiment (Table 2). The right-hand side comprises the combined apparent turbulent tendency of $T - L_v/c_p\, q_l - L_i/c_p\, q_i$ from which the related turbulent flux can be calculated.

Adding eqs (43) and (44) to eq. (42) and observing relations (45)–(47) yields:

$$\begin{aligned}
&\left.\frac{\partial q_v}{\partial t}\right|_{\mathrm{diff}} + \left.\frac{\partial q_l}{\partial t}\right|_{\mathrm{diff}} + \left.\frac{\partial q_i}{\partial t}\right|_{\mathrm{diff}} \\
&\quad = \left.\frac{\partial q_v}{\partial t}\right|_{\mathrm{diff}}^{\mathrm{turb}} + \left.\frac{\partial q_l}{\partial t}\right|_{\mathrm{diff}}^{\mathrm{turb}} + \left.\frac{\partial q_i}{\partial t}\right|_{\mathrm{diff}}^{\mathrm{turb}}.
\end{aligned} \tag{50}$$

The tendencies on the left-hand side are available from the 1-yr experiment (Table 2). Thus the tendency due to the combined turbulent transport of $q_v$, $q_l$ and $q_i$ (right-hand side of eq. 50) can be calculated. The corresponding turbulent flux is obtained from vertical integration.

Note: Only the sum of the turbulent transport tendencies on the right of (49) and (50) can be calculated. This is because of the implementation of the diffusion scheme, where the turbulent transport is formulated for total water $q_t = q_v + q_l + q_i$ and liquid water static energy $s_l = gz + c_pT - L_vq_l - L_iq_i$ (ECMWF, 2007). It was decided to treat the turbulent transport of $q_l$ and $q_i$ as negligible. This is consistent with the implementation of the diffusion scheme, where the profiles of $q_l$ and $q_i$ are not altered by turbulent transport except for condensation due to supersaturation. Hence the turbulent fluxes calculated through vertical integration (see eq. 27) of the turbulent tendencies (49) and (50) are considered as the kinematic turbulent fluxes of temperature $F^T_{\mathrm{diff}}$ and specific humidity $F^{q_v}_{\mathrm{diff}}$ due to the diffusion scheme.

## References


Arakawa, A. 2004. The cumulus parametrization problem: past, present, and future. *J. Climate* **17**, 2493–2525.

Arpe, K., Brankovic, C., Oriol, E. and Speth, P. 1986. Variability in time and space of energetics from a long series of atmospheric data produced by ECMWF. *Beitr. Phys. Atmos.* **59**, 321–355.

Bhatla, R., Mohanty, U., Raju, P. and Madan, O. 2004. A study on dynamic and thermodynamic aspects of breaks in the summer monsoon over India. *Int. J. Climatol.* **24**, 341–360.

Boer, G. J. 1975. Zonal and eddy forms of the available potential energy equations in pressure coordinates. *Tellus* **27**, 433–443.

Boer, G. J. and Lambert, S. 2008. The energy cycle in atmospheric models. *Clim. Dyn.* **30**, 371–390.

ECMWF 2007. IFS documentation (CY31r1). ECMWF, http://www.ecmwf.int/research/ifsdocs/CY31r1/index.html.

Falk, G. and Ruppel, W. 1976. *Energie und Entropie. Eine Einführung in die Thermodynamik*, Springer, Berlin - Heidelberg - New York, 408.

Fortelius, C. 1995. Inferring the diabatic heat and moisture forcing of the atmosphere from assimilated data. *J. Climate* **8**, 224–239.

Gill, A. E. 1982. *Atmosphere-Ocean Dynamics*, Volume 30: International Geophysics Series, Academic Press, Orlando, Florida 662.

Haimberger, L. and Hantel, M. 2000. Implementing convection into Lorenz's global cycle. Part II: a new estimate of the conversion rate into kinetic energy. *Tellus* **52A**, 75–92.

Hamelbeck, F., Haimberger, L. and Hantel, M. 2001. Convection in PIDCAP. Part I: Evaluating LAM convection. *Meteorol. Atmos. Phys.* **77**, 85–98.

Hantel, M. and Baader, H. R. 1978. Diabatic heating climatology of the zonal atmosphere. *J. Atmos. Sci.* **35**, 1180–1189.

Hantel, M. and Haimberger, L. 2000. Implementing convection into Lorenz's global cycle. Part I: gridscale averaging of the energy equations. *Tellus* **52A**, 66–74.

Hantel, M., Ehrendorfer, M. and Haimberger, L. 1993. A thermodynamic diagnostic model for the atmosphere. Part II: the general theory and its consequences. *Meteorol. Z., N.F.* **2**, 255–271.

Hantel, M., Haimberger, L. and Hamelbeck, F. 2001. Convection in PIDCAP Part II: DIAMOD—a standard for diagnosing convective quantities. *Meteorol. Atmos. Phys.* **77**, 185–204.

Hortal, M. 2002. The development and testing of a new two-time-level semi-Lagrangian scheme (SETTLS) in the ECMWF forecast model. *Quart. J. Roy. Met. Soc.* **128**, 1671–1687.

Hoskins, B. J., Hsu, H. H., James, I. N., Masutani, M., Sardeshmukh, P. D. and co-authors. 1989. *Diagnostics of the global atmospheric circulation*, WCRP-27. WMO, 217.

Johnson, D. 2000. Entropy, the Lorenz Energy Cycle, and Climate. In: *General Circulation Model Development. Past, Present, and Future*, (ed. D. Randall), Volume 70: International Geophysics Series, Chapter 22, 659–720. Academic Press, San Diego, California; London.

Kalnay, E., Kanamitsu, M., Kistler, R., Collins, W., Deaven, D., and co-authors. 1996. The NCEP/NCAR 40-year reanalysis project. *Bull. Amer. Meteorol. Soc.* **77**, 437–471.

Li, L., Ingersoll, A. P., Jiang, X., Feldman, D. and Yung, Y. L. 2007. Lorenz energy cycle of the global atmosphere based on reanalysis datasets. *Geophys. Res. Lett.* **34**, L16813.

Lorenz, E. N. 1955. Available potential energy and the maintenance of the general circulation. *Tellus* **7**, 157–167.

Lorenz, E. N. 1967. *The Nature and Theory of the General Circulation of the Atmosphere*, WMO–No.218.TP.115. World Meteorological Organization, 161.

Newell, R. E., Vincent, D. G., Dopplick, T. G., Ferruzza, D. and Kidson, J. W. 1970. The energy balance of the global atmosphere. In: *The Global Circulation of the Atmosphere* (ed. G. A. Corby). Roy. Met. Soc., London, 42–90.

Oort, A. H. 1964. On estimates of the atmospheric energy cycle. *Mon. Wea. Rev.* **92**, 483–493.

Oort, A. H. 1983. *Global Atmospheric Circulation Statistics, 1958–1973*, Volume 14: NOAA Professional Paper. U.S. Department of Commerce/NOAA, 180.

Oort, A. H. and Peixóto, J. P. 1983. Global angular momentum and energy balance requirements from observations. *Adv. Geophys* **25**, 355–490.

Oort, A. H. and Rasmusson, E. M. 1971. *Atmospheric Circulation Statistics*, Volume 5: NOAA Professional Paper. U.S. Department of Commerce/NOAA, 323.

Peixóto, J. P. and Oort, A. H. 1992. *Physics of Climate*, American Institute of Physics, New York, 520.

Ritchie, H., Temperton, C., Simmons, A., Hortal, M., Davies, T., and co-authors. 1995. Implementation of the semi–Lagrangian method in a high–resolution version of the ECMWF forecast model. *Mon. Wea. Rev.* **123**, 489–514.

Rosen, R. D. 1999. The global energy cycle. In: *Global Energy and Water Cycles* (eds K. A. Browning and R. J. Gurney). Chapter 1.1, Cambridge University Press, Cambridge, 1–9.

Siegmund, P. 1994. The generation of available potential energy, according to Lorenz' exact and approximate equations. *Tellus* **46A**, 566–582.

Simmons, A. J. and Burridge, D. M. 1981. An energy and angular–momentum conserving vertical finite-difference scheme and hybrid vertical coordinates. *Mon. Wea. Rev.* **109**, 758–766.

Stull, R. B. 1988. *An Introduction to Boundary Layer Meteorology*. Atmospheric Sciences Library. Kluwer Academic Publishers, Dordrecht, 666.

Uppala, S. M., Kållberg, P. W., Simmons, A. J., Andrae, U., da Costa Bechtold, V., and co-authors. 2005. The ERA-40 re-analysis. *Quart. J. Roy. Meteor. Soc.* **131**, 2961–3012.

van Mieghem, J. 1973. *Atmospheric Energetics*, Oxford Monogr. on Meteorology. Clarendon Press, Oxford, 306.

Yanai, M. and Johnson, R. H. 1993. Impacts of cumulus convection on thermodynamic fields. In: *The Representation of Cumulus Convection in Numerical Models* (eds K. A. Emanuel and D. J. Raymond). Volume 24: Meteorological Monographs, American Meteorological Society, Boston, Massachusetts , 39–62.